

STRUCTURE AND PROPERTIES OF
COPPER INFILTRATED IRON

by

TIBOR KRANTZ

A THESIS SUBMITTED IN PARTIAL FULFILMENT OF
THE REQUIREMENTS FOR THE DEGREE OF
MASTER OF APPLIED SCIENCE

in the Department

of

METALLURGY

We accept this thesis as conforming to the
required standard

Members of the Department of Metallurgy

THE UNIVERSITY OF BRITISH COLUMBIA

April, 1964

In presenting this thesis in partial fulfilment of the requirements for an advanced degree at the University of British Columbia, I agree that the Library shall make it freely available for reference and study. I further agree that permission for extensive copying of this thesis for scholarly purposes may be granted by the Head of my Department or by his representatives. It is understood that copying or publication of this thesis for financial gain shall not be allowed without my written permission.

Department of Metallurgy

The University of British Columbia,
Vancouver 8, Canada.

Date April 27, 1964

ABSTRACT

Two-phase composites have been prepared by infiltrating sintered iron compacts with liquid copper. The effects have been studied of iron particle size, matrix mean free path, and the volume fraction and micro-hardness of the iron-rich constituent, on the tensile properties of composites.

It has been found that the strength of the composites is related to the amount of solution hardening of the iron component during infiltration.

The results of tensile tests have suggested that the hardness of the iron-rich constituent is the dominant factor controlling yield strength, ultimate tensile strength and elongation. However, the ultimate strength has been found to depend also on the volume fraction of the hard constituent, and elongation has also been found to be a function of the interface area.

ACKNOWLEDGEMENTS

The author wishes to thank his research director, Dr. J.A. Lund for his advice and assistance in the interpretation of this research. He also wishes to express his thanks to Drs. L.C. Brown and E. Teghtsoonian and to other faculty members and fellow graduate students for helpful discussion of certain points in this thesis.

The National Research Council Grant No. A-1463, Defence Research Board Grant No. 7501-02 and Canadian Western Pipe Mills Limited Fellowship in Metallurgy provided financial assistance. This assistance is gratefully acknowledged.

TABLE OF CONTENTS

	<u>Page</u>
I. INTRODUCTION AND SCOPE	1
REVIEW OF LITERATURE	3
1. Properties of Two-Phase Structures.	3
2. Previous Work with Iron-Copper Composites	6
II. EXPERIMENTAL PROCEDURE	8
1. Materials	8
2. Specimen Preparation	9
a. Compacting	9
b. Sintering	10
c. Infiltration	11
3. Density Measurement.	12
4. Tensile Testing	13
5. Metallography	14
a. Microhardness.	15
b. Constitution, Mean Free Path, Particle Size.	15
III. EXPERIMENTAL RESULTS	17
1. Infiltration Time	17
2. Infiltration Temperature.	24
3. Volume Fraction of Infiltrant	30
4. Particle Size of Iron	33
5. Additional Experimental Results	37
a. Constitution	37
b. Lattice Parameter of the Iron-Rich Constituent	37
c. Cooling Rate Effects	38
d. Properties of Bulk Copper-Rich Alloy	38
e. Relative Plastic Deformation of the Two Constituents	39
f. Effect of Gas Pressure in Infiltration.	40
IV. DISCUSSION	42
1. Porosity in Composites.	42
2. Growth in Iron Constituent Particles.	44
3. Effect of Various Factors on the Tensile Properties of Composites.	46
a. Matrix Mean Free Path and Interparticle Spacing of Iron.	46
b. Volume Fraction of Constituent	47
c. Hardness of the Iron Constituent	48
4. Summary	52
V. CONCLUSIONS.	54
VI. APPENDICES	55
VII. BIBLIOGRAPHY	60

LIST OF FIGURES

<u>Number</u>		<u>Page</u>
1	Iron-Copper Equilibrium Diagram	1a
2	Effect of Infiltration Time on Iron Particle Size (Inf. Temp. 1150°C).	19
3	Effect of Infiltration Time on Microhardness of the Two Constituents (Inf. Temp. 1150°C).	20
4	Effect of Infiltration Time on Strength of Copper Infiltrated Iron (Inf. Temp. 1150°C).	21
5	Sintered Iron Skeleton, 300 X	22
6	Specimen Infiltrated 10 min. at 1150°C, 300 X	22
7	Specimen Infiltrated 120 min. at 1150°C, 300 X.	23
8	Specimen Infiltrated 420 min. at 1150°C, 300 X.	23
9	Effect of Infiltration Temperature on Iron Particle Size (Inf. Time 10 min.)	26
10	Effect of Infiltration Temperature on Microhardness of the Two Constituents (Inf. Time 10 min.)	27
11	Effect of Infiltration Temperature on Strength of Copper Infiltrated Iron (Inf. Time 10 min.)	28
12	Grain Boundary Penetration of Cu into Fe, 800 X	29
13	Mean Free Path versus Volume Percent of the Copper- Rich Constituent.	32
14	Mean Free Path versus Iron Particle Size.	35
15	Elongation versus Surface Area of Iron-Rich Particles	36
16	Fracture after Large Plastic Deformation, 150 X	41
17	Brittle Fracture, 300 X	41

LIST OF TABLES

<u>Number</u>		<u>Page</u>
1	Infiltration Time.	18
2	Infiltration Temperature	25
3	Volume Fraction of Infiltrant.	31
4	Particle Size.	34

STRUCTURE AND PROPERTIES OF COPPER INFILTRATED IRON

I. INTRODUCTION AND SCOPE

Infiltration (applied to metals) is a process by which the pores of a metal powder compact are filled with a relatively low melting liquid metal through the action of capillary forces. This process yields a composite material with a combination of physical and mechanical properties of the components which cannot be achieved by any other method of processing.

The technique is considered applicable to systems¹ where the components have:

- a) widely different melting points
- b) limited mutual solubilities
- c) good "wetting characteristics" (defined below)
- d) no intermetallic compound formation which might interfere with further infiltration

There are few binary metallic systems which satisfy these requirements fully, and among them the iron-copper system is probably the best known.

The melting points of pure iron and copper are 1536°C and 1083°C respectively.

The equilibrium diagram for the Fe-Cu system² is given in Figure 1. At 1100°C the solid solubility of copper in iron is 8.5% and this proportion varies only slightly over the range of temperature with which the present investigation is mainly concerned. The solubility of iron in copper at 1094°C is 4%, but decreases to 2.3% as a result of a peritectic reaction on cooling

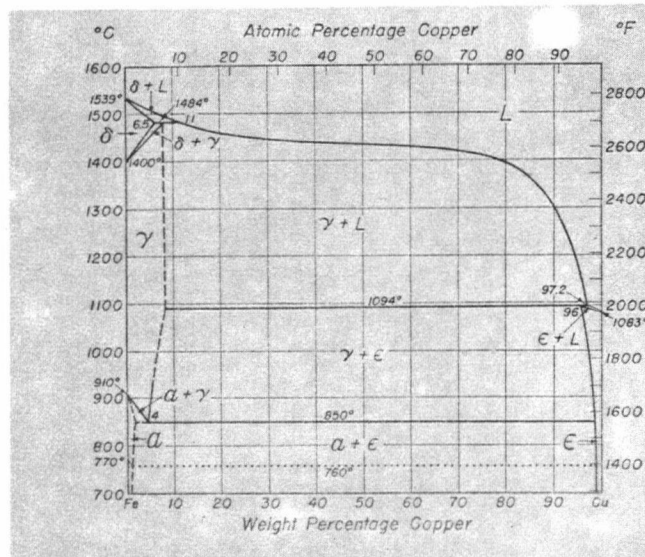


Figure 1. Iron-Copper Equilibrium Diagram

through that temperature. Above this transformation point the solubility increases again with temperature.

It is also seen from the diagram that no intermetallic compounds occur in the iron-copper system.

The "wetting characteristics" of this system are good. The wetting angle of molten copper with solid iron is reported to be zero³. The dihedral angle, a parameter determining the intergranular penetration of the solid by the liquid is 27°³.

According to Kingery⁴ the following surface energy relationship is required for wetting and densification of a porous body by a liquid infiltrant

$$\gamma_{SV} > \gamma_{LV} > \gamma_{SS} > 2\gamma_{SL}$$

where the subscripts V, L and S refer to vapor, liquid and solid respectively.

In the case of Fe-Cu the following numerical values can be substituted

$$(\gamma_{SV} = 1950)^5 > (\gamma_{LV} = 1269)^6 > (\gamma_{SS} = 850)^7 > 2(\gamma_{SL} = 430)^8 \frac{\text{erg}}{\text{cm}^2}$$

According to these values the solid-vapor interface is eliminated first by covering of the iron with molten copper; in the second stage the pores formed between the copper-coated iron particles are filled. The third stage, grain boundary penetration, is apparently not favourable. However, since γ_{SS} is affected by the angle of the boundary and by the stress distribution in the system, under certain conditions or in certain regions this third stage can occur also.

The structures of artificial two-phase composites which can be prepared by infiltration can be closely controlled with respect to phase distribution and other parameters. Thus they lend themselves well, in principle, to studies of the deformation behaviour of mixtures of ductile phases. It was primarily with the object of learning more about the properties of such mixtures that the present study was undertaken. Moreover, it was hoped that it might be possible to explain some of the inconsistencies in the results of previous investigations with copper-infiltrated iron compacts, since such materials are important commercially.

REVIEW OF LITERATURE

1. Properties of Two-Phase Structures

The mechanism of plastic deformation in a two-phase alloy is considerably more complex than in a polycrystalline single phase alloy. Besides the usual obstacles to dislocation movement we find the interfaces and the second phase itself as additional barriers to slip in the matrix. Their effect on the passage of dislocations depends on the degree of misfit of the two lattices, on the difference between the elastic properties of the two phases and on the amount and distribution of the two phases. These parameters vary from system to system, and may be varied within one system by the conditions of experiment. In metallurgical investigations it is common practice to correlate the micro-structure with the deformation behaviour of an alloy and to determine the factors responsible for a certain effect. The most often quoted parameters characterizing a two phase structure are:

- a) mean free path between second-phase particles
- b) interparticle spacing between second-phase particles
- c) volume percent of the second phase
- d) hardness of the two phases

These parameters have been examined by others in detail for various two-phase systems, and relationships have been derived between them and the yield strength, fracture strength and ductility of composites.

Gensamer⁸, studying the structures of slow cooled and spheroiditic steels, proposed the relationship

$$\sigma_y = -A \log (\text{MFP}) + B$$

indicating that the yield stress depends on the log of the mean free path, MFP, through the continuous phase (ferrite) from one hard phase (cementite) particle or lamella to another.

Edelson and Baldwin⁹ have studied the effect of various second phase additions on the yield strength of copper. They conclude that only those particles strengthen copper which form a firm bond with the matrix and that in such cases the yield strength again depends upon MFP.

Krock¹⁰ found that in W-NiFeW composites the deformation characteristics were independent of MFP.

The interparticle spacing criterion appears to play an important role in dispersion hardening.

Gregory and Grant¹¹ working with fine oxide dispersoids in aluminum found that the strength was proportional to the reciprocal of the oxide particle spacing.

The comparative value of Gregory's results with other two-phase structures is doubtful since dispersion-strengthened alloys form a special class of materials involving low volume fractions and extremely fine particles of what is usually a non-metallic dispersoid. Due to the small dimensions of these particles the interparticle distance is actually very close to the mean free path.

There have been many attempts to correlate the mechanical properties of composites with the volume fraction of the harder phase. The results reported in this regard are very controversial.

Pines and Sukhinin¹² derived mathematically a relationship between strength p , and constitution

$$p = p_1 (1-x)^2 + p_2 x^2 + 2p_{12}x(1-x)$$

where x is the volume fraction of the matrix, and p_1 , p_2 and p_{12} respectively the strengths of the discontinuous phase, the matrix and the interface. Their experimental results obtained at the Cu rich end of the Fe-Cu system appeared to be in good agreement with the theoretical derivation.

Teodorovich¹³ in experiments with brass infiltrated iron found that when the brass content was decreased from 39 to 20% the yield strength increased from 21,000 psi to 57,000 psi while the elongation to fracture decreased from 8 to 4%.

Edelson⁹ found that ductility, unlike YS, was a function of volume fraction of the phases.

Kimura¹⁴ reported that the fracture strength of iron infiltrated with a Pb-Sn alloy remained essentially constant from 25% to 80% of iron and was close to the bulk strength of the matrix. Above 90% iron the composite strength increased.

Goetzel¹⁵ with the Fe-Cu system found no change in composite YS and UTS in the range of 72-82% iron, but above that there was a sudden increase in YS from 28,000 to 53,000 psi.

Krock¹⁰ observed that the deformation characteristics of W-NiFeW composite were independent of the volume fraction, at least in the range of 20-42% of the matrix phase.

Previous Work with Iron-Copper Composites

A significant volume of research has previously been carried out on Fe-Cu composites because of the favorable infiltration characteristics of the Fe-Cu system and because of its commercial importance and potentialities.

In what follows no distinction will be made between the processes of infiltration and liquid phase sintering, since the two are essentially identical with the same mechanism and driving force involved.

The infiltration of iron compacts with copper (and liquid phase sintering of iron-copper powder mixtures) began to attract considerable interest in the late nineteen forties after some initial studies in Germany during World War II.

Kopecki¹⁷ and Kelley¹⁸ (1946), Goetzel¹⁵ and Northcott¹⁹ (1947) and Smith²⁰ (1950) investigated the procedures of infiltration and the effect of alloying additions and heat treatment on copper-infiltrated iron with the purpose of establishing conditions to obtain the best combination of mechanical properties. In the second stage of development the basic mechanism of infiltration became the main target of studies by Elliot¹ (1955), Kingery⁴ (1959), Edelson⁹ and Whalen³ (1962).

Although it was recognized from the start^{1,15,19,21} that alloying between copper and iron took place, the strength increase due to infiltration was at first attributed to "cementing" or a "heavy-alloy mechanism" similar to the one operating in carbide-cobalt alloys (Goetzel^{15,23}, Northcott¹⁹, and Schwartzkopf²⁴). According to this mechanism the hard particles round off by solution and reprecipitation through the liquid phase and after complete solidification the two phases are bonded by cohesive forces only. This mechanism is still a subject of controversy in the carbide-cobalt system itself.

As shown by Gurland²⁵, in the WC-Co system there is a large solubility of the carbide in cobalt (38% by weight above the melting point, 17% below it) an appreciable temperature dependence of the solubility, and a zero dihedral angle causing very large changes in the microstructure on cooling even by quenching. While there is no continuous WC skeleton at elevated temperatures, it is continuous at ordinary temperature.

In the case of Fe-Cu these parameters are entirely different and no appreciable structure change is expected to occur during cooling.

In recent years the emphasis has moved from the heavy alloy mechanism explanation to a solution hardening argument. Northcott as early as 1947 noticed diffusion layers in the iron particles, however, he did not attribute any significance to them.

Elliot¹ (1955) recognized that the diffusion of Cu into Fe would evidently bring about a change in the mechanical properties of the iron and that the degree of change would depend upon the amount of copper dissolved.

Rennhack²¹ and Teodorovich^{13,22} were the first (1961) to advance solution hardening as the basic mechanism of strengthening. Rennhack observed the heavy-alloy mechanism operating after saturation of iron with copper, which was contrary to observations of others.

Edelson and Baldwin⁹ stated that all "second phases" (metallic, non-metallic and voids) embrittle a matrix because of stress concentration, provided the second-phase is significantly harder than the matrix. One of the composites they examined and found brittle was iron-copper. Other workers have observed good ductilities with this system which indicates that the brittleness is not an inherent property of the composite but depends on the actual microstructure.

The alloying of the Fe component of the Fe-Cu system has been found to have an important effect on the final properties of the infiltrated product. Schwartzkopf²⁴ reported that the addition of 0.25% carbon to iron increased the YS of an as-infiltrated product from 61,200 to 72,900 psi. and the UTS from 67,500 to 76,100 psi.

At present, in spite of the extended commercial use and practical development of iron-copper composites, the structure and the origins of the properties of these alloys are still matters of considerable controversy.

The metallographic structures of iron-copper composites have been examined by almost every worker in the field, but no one has attempted an even qualitative evaluation of the changes occurring during infiltration, with the exception of Frantzevich²⁷, who measured various parameters, but arrived at no conclusions based on these measurements.

II. EXPERIMENTAL PROCEDURE

1. Materials

The materials employed in these experiments were:

Iron Powder

A 100 lb. lot of Armco Iron was atomized and supplied as spherical powders by Federal Mogul Co. for this investigation. It was shipped in an airtight container with a desiccant.

The nominal composition of the powder was:

	C	Mn	P	S	Si
%	0.012	0.017	0.005	0.025	trace

The powder was separated into 5 particle-size fractions using a standard screening procedure.

Sieve fraction (Tyler)	Estimated average particle size (micron)
-100 +150	127
-150 +200	89
-200 +270	63
-270 +325	48
-325	25

The sieved fractions were placed into polyethylene bags which were filled with nitrogen and sealed off until required. Only the finest fraction (=325 mesh) underwent any visible oxidation during the experimental period.

Metallographic examination of the powders showed that the particles were nearly perfect spheres although many were hollow. No agglomeration of the particles was observed.

Copper

Electrolytic Tough Pitch copper (copper - 99.92% min., oxygen - 0.04%) was obtained in the form of rod, 3/8 inch in diameter. Lengths of 2 1/2 inch were employed for infiltration. The rod was supplied by Western Copper Mills Limited (Noranda).

2. Specimen Preparation

a. Compacting

The majority of the iron compacts were prepared by hydrostatic compaction. This method was preferred to conventional pressing in rigid dies because of the more uniform density of the product.

Since the iron powder particles were of spherical shape and were used in narrow size fractions, compactibility was very poor and the addition of a binder, a 1:1 mixture of Acrysol and NH_4OH , was added in the ratio of 1 drop per 30-40 g of powder, and thoroughly mixed with the iron by hand just before compacting. The mixture was placed in a rubber tube 4" long, 12 mm. O.D., with 2 mm. wall thickness, and sealed at one end with a rubber stopper. After filling, the other end of the rubber tube was also stoppered and tied with a copper wire. Three such bags were filled and placed at one time in a steel hydrostatic pressure cylinder of 2" I.D. and depth 6", which was then filled with oil. The contents of the pressure vessel were compressed at 20,000 to 30,000 psi. The compacts were 3.5" long and 0.4" diameter. Despite the presence of a binder the compacts were very fragile and many collapsed during handling.

Some specimens were prepared from uncompacteds powders. In this case, loose powder was placed in a 0.3" ϕ molybdenum tube with a closed end and the whole assembly was in turn enclosed into a quartz tube and sintered as described in the following section.

b. Sintering

Sintering was carried out in order to give the compact sufficient strength to withstand further handling and machining.

The furnace used for both sintering and infiltration was an electric resistance type, containing six, 12 mm. diameter "Globar" (SiC) elements placed vertically in a circle of 5.5" diameter. The uniform hot zone in the centre (gradient less than 10 degrees Centigrade) was found to be 3.5" long. Temperature control was provided by a Honeywell controller with a Pt-Pt 10 Rh thermocouple installed in the centre of the uniform hot zone. The setting of the controller was adjusted daily according to the actual temperature measured

inside a quartz tube similar to the one used in the experiments. The maximum temperature variation inside this tube was found to be $\pm 4^{\circ}\text{C}$ at 1150°C .

A compacted billet (or the molybdenum tube containing loose powder) was placed at the bottom of a sealed quartz tube, 20 mm. I.D., which was lowered vertically into the furnace. All sintering treatments were carried out at 1150°C for 10 minutes, with a flow of cracked ammonia through the container. The reducing gas inlet and an outlet were positioned in such a way that the compact was in the actual gas stream. The temperature of the specimen reached the pre-set value approximately 5 minutes after loading.

After sintering, the tube and contents were pulled out from the furnace and allowed to cool in the air with cracked ammonia still flowing.

c. Infiltration

Infiltration took place in a 12 mm. I.D. quartz tube, sealed at one end. A 12-15 g piece of copper rod, plus some iron powder (approximately 1.5 g) were charged into the bottom of the tube. The iron compact, by means of a small hole drilled into it near one end was suspended from a 12" long tungsten wire, to the upper end of which was attached a 1" x 0.3" steel cylinder. The latter cylinder served as a core between two permanent magnets placed outside the quartz tube. By moving these magnets along the tube the core and the attached wire and powder compact could be lowered or raised inside the tube. The upper (open) end of the tube was connected to a vacuum forepump and the system was pumped for several minutes to obtain a stable vacuum of approximately 65 microns.

After evacuation the tube was lowered vertically into the furnace with the bottom supported 1 1/2" below the centre of the uniform heat-zone. The specimen to be infiltrated was then in the protruding part of the tube. The tube was allowed to come to thermal equilibrium during which the copper melted and became saturated with iron from the iron powder addition. This saturation was necessary in order to prevent erosion of those portions of the compact which first came in contact with the liquid metal¹.

After 10 minutes the powder compact was lowered to the bottom of the tube, submerged approximately 1/2 inch into the molten pool, where it was held for a measured time, ranging from 10 min. to 420 min., and was then withdrawn rapidly into the cold top half of the tube. The temperature of infiltration was varied from 1100° to 1370°C.

When the infiltrated specimen had cooled below visible red heat (approx. 650°C) the whole tube was pulled out from the furnace and quenched in water.

3. Density Measurements

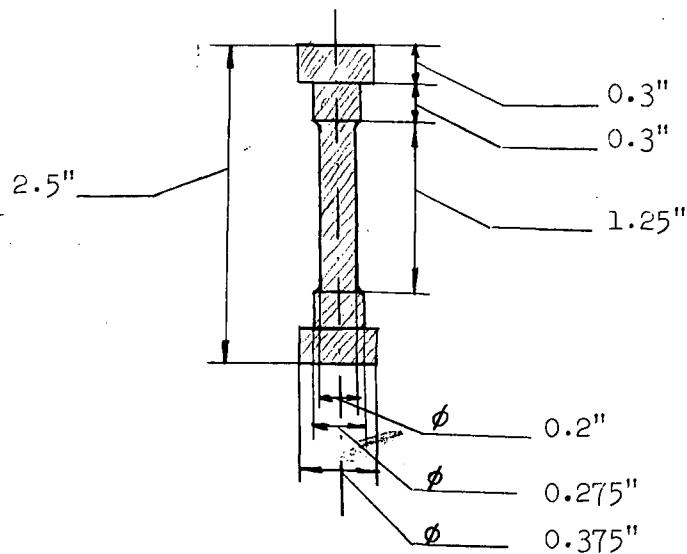
Density measurements were carried out on all specimens after sintering and after infiltration.

Sintered iron specimens were machined into perfect cylinders, their physical dimensions and their weights were measured, and the specific weights were then calculated. Density was recorded as a percent of the theoretical, taken as 7.87 g/cc for iron.

The density of infiltrated specimens was obtained by liquid immersion techniques. Carbon tetrachloride was used as the liquid medium because of its relatively high specific gravity (1.54 g/cc) and good wetting characteristic. The calculation of the theoretical density was based on the sintered density of the given specimen. It was assumed, and later proven through chemical and metallographic analysis, that the Fe/Cu volume ratio after infiltration was the same as the Fe/pore ratio in the sintered specimen. The density of copper was taken as 8.94 g/cc. for purposes of calculating densities as a percentage of theoretical.

4. Tensile Testing

All infiltrated compacts were machined into tensile specimens of the shape and dimensions shown below.



Specimens were tested in tension on an Instron tensile testing machine, using grips specially made for the button-head specimens. All tests were carried out at ambient temperature. The strain rate used in most cases was 0.2 min^{-1} although 0.02 min^{-1} was used in a few instances. There were usually 3 specimens tested for any given condition (Appendix II).

The load-elongation curves were recorded. The maximum load was converted to ultimate tensile strength, and yield strength was determined by using a 0.2% offset.

Elongations were measured on 1" gauge lengths, marked on the specimens before testing.

5. Metallography

One specimen for each condition was examined metallographically. Three sections were mounted- one transverse taken from the top shoulder, and two longitudinal, exposing both halves of the specimen fracture.

In order to retain the sharp fracture-edge and to prevent any relief formation due to the hardness difference of the phases, lapping was carried out with 6μ and 1μ diamond. A final light polish was provided by Linde B alumina.

The polished specimens were etched in 4% nitric acid in ethanol which produced various degrees of brownish coloration in the Fe-rich constituent. The darkness of this coloring was found to be roughly proportional to the amount of copper in the iron and served as a qualitative measure of the extent of diffusion.

The Cu-rich matrix was etched when required with a solution of 5 parts of concentrated NH_4OH , 3 parts of 3 per cent H_2O_2 and 5 parts H_2O .

a. Microhardness

Microhardness measurements were made on a Tukon tester with a 145° diamond pyramid indenter. Two loads, 50 g and 10g, were used, but one load only was used in a given series of experiments. Mean hardnesses were based on measurements of 6 to 12 indentations depending on the observed scatter. In the case of the iron-rich constituent wherein the hardness differed considerably with distance from the matrix, care was taken to make indentations on many particles of the various shadings of etched color to obtain an average hardness.

b. Constitution, Mean Free Path, Particle Size

The measurement of these parameters was carried out by standard lineal analysis²⁸ on a Tukon tester equipped with a filar eye piece and a transiting stage with vernier adjustment.

Traverses on the specimen were made in three different directions. During a traverse the number of iron particles was counted, and the total length of the line and the lengths of the copper intercepts were measured. Transits were made over 250 to 300 iron particles for each sample in order to obtain a reliable average.

The constitution determination is based on the premise that the ratio of intercepts of the two constituents on a random line in a random metallographic section, $\frac{l_{\text{Cu}}}{l_{\text{Fe}}}$, gives the actual volume ratio of the constituents²⁸.

The matrix mean free path, i.e. the mean distance between the Fe particles, was obtained by dividing the total length of Cu intercepts with the

number of iron particles intercepted in the total traverse length; $MFP = \frac{l_{Cu}}{N_{Fe}}$

The average iron-particle size was determined similarly, i.e.

$$d_{Fe} = \frac{L_t - l_{Cu}}{N_{Fe}} \quad \text{where}$$

L_t is the total length of the line of travel

l_{Cu} is the length of Cu intercepts

N_{Fe} is the number of iron particles traversed

It should be noted that whereas the mean free path obtained by this method is equal to the true volumetric mean free path²⁸ the particle size d_{Fe} is only two-thirds of the true particle diameter²⁹ for particles of uniform size. In the case of non-uniform particles, the mean size measured metallographically is also a function of the size distribution of the particles. The larger is the size difference between the particles the greater is the probability of a small particle being totally above or below the plane of metallographic examination. Since the apparent particle size measured metallographically is inversely proportional to the number of particles sectioned by a random plane, a reduction in the number of the particles would lead to an increase in the apparent size. Thus, in the case where some particles of initially uniform size, grow at the expense of others during infiltration, an apparent mean particle-size increase is observed metallographically. In fact, the true mean diameter is decreasing, at least up to the point where some particles disappear completely.

However, since this study was concerned only with relative changes of the parameters, the diameter values used throughout this work have not been corrected to allow for the above effects.

III. EXPERIMENTAL RESULTS

All experimental data and results are summarized in Appendices II and III.

1. Infiltration Time

Specimens prepared from 200 x 270 mesh iron powder pressed at 30,000 psi. were infiltrated for 10, 60, 120, 200, 300 and 420 minutes at 1150°C. The parameters of the microstructure and the mechanical properties of representatives of these infiltrated specimens are given in Table 1. The reproducibility of tensile test results for each of the conditions represented in Table 1. may be observed in Appendix II. Only those specimens for which complete metallographic studies were carried out have been included in Table 1.

The following observations can be made on the basis of these measurements:

- a. The infiltrated density (98.2% of theoretical on the average) is independent of the time of infiltration.
- b. The Fe/Cu ratio, based on metallographic analysis is also essentially constant.
- c. The apparent iron-particle size increases rapidly in the early periods of infiltration (Figure 2). This growth later slows down and after 3 hours has essentially ceased.
- d. The mean free path also appears to increase with time as a natural consequence of iron-particle growth- however, the effect of the initial density, which varied to a certain degree, is superimposed on this effect and the trend is not obvious.
- e. The microhardness of the copper-rich matrix is essentially constant with infiltration time, whereas the hardness of the iron-rich constituent increases rapidly and linearly up to ~ 3 hours where it suddenly levels off (Figure 3).

TABLE 1

Infiltration Time (Inf. at 1150°C)
200 x 270 Iron Powder

Inf. Time min.	Start Dens. %	Inf. Dens. %	Cu content		Ratio Met/Calc	Fe Part Size		Ratio Met/Sieve	Int. Part. Space μ	Mean Free Path μ	Hardness ^{AA}		YS psi	UTS psi	E %	Spec. No.
			Calc. %	Met. %		Sieve μ	Met μ				Fe VHN	Cu VHN				
0	70.7	-	-	74.6 ^A	1.05	63	43.8	0.70	58.7	14.9	103	-	19,000 ^{AAA}	38,500 ^{AAA}	45 ^{AAA}	40
10	77.7	98.0	22.3	19.6	0.88	63	48.7	0.77	60.5	11.8	122	118	20,000	39,100	9.4	28
60	78.5	98.4	21.5	21.3	0.99	63	50.2	0.80	63.9	13.7	137	117	28,200	45,500	7.0	31
120	77.3	97.8	22.7	19.9	0.88	63	52.6	0.83	65.7	13.1	169	110	42,000	52,800	5.0	67
200	79.5	98.3	20.5	19.6	0.96	63	53.5	0.85	66.5	13.0	204	117	54,700	62,700	3.5	25
300	77.2	98.5	22.8	25.4	1.11	63	53.9	0.86	72.2	18.3	203	112	55,300	64,700	4.0	89
420	75.0	98.2	25.0	24.0	0.96	63	52.9	0.84	69.7	16.8	206	111	56,100	66,900	1.0	59

Abbreviations in the column headings for Tables 1 to 4

Inf. - infiltration

Dens. - density

Calc. - value calculated from density measurements

Met. - value obtained through metallographic measurements

Int. part. space. - inter particle spacing,

^A Fe content obtained metallographically

^{AA} 50 g load

^{AAA} Metals Handbook 1948, p. 432 "Dead Soft"

Armco Iron

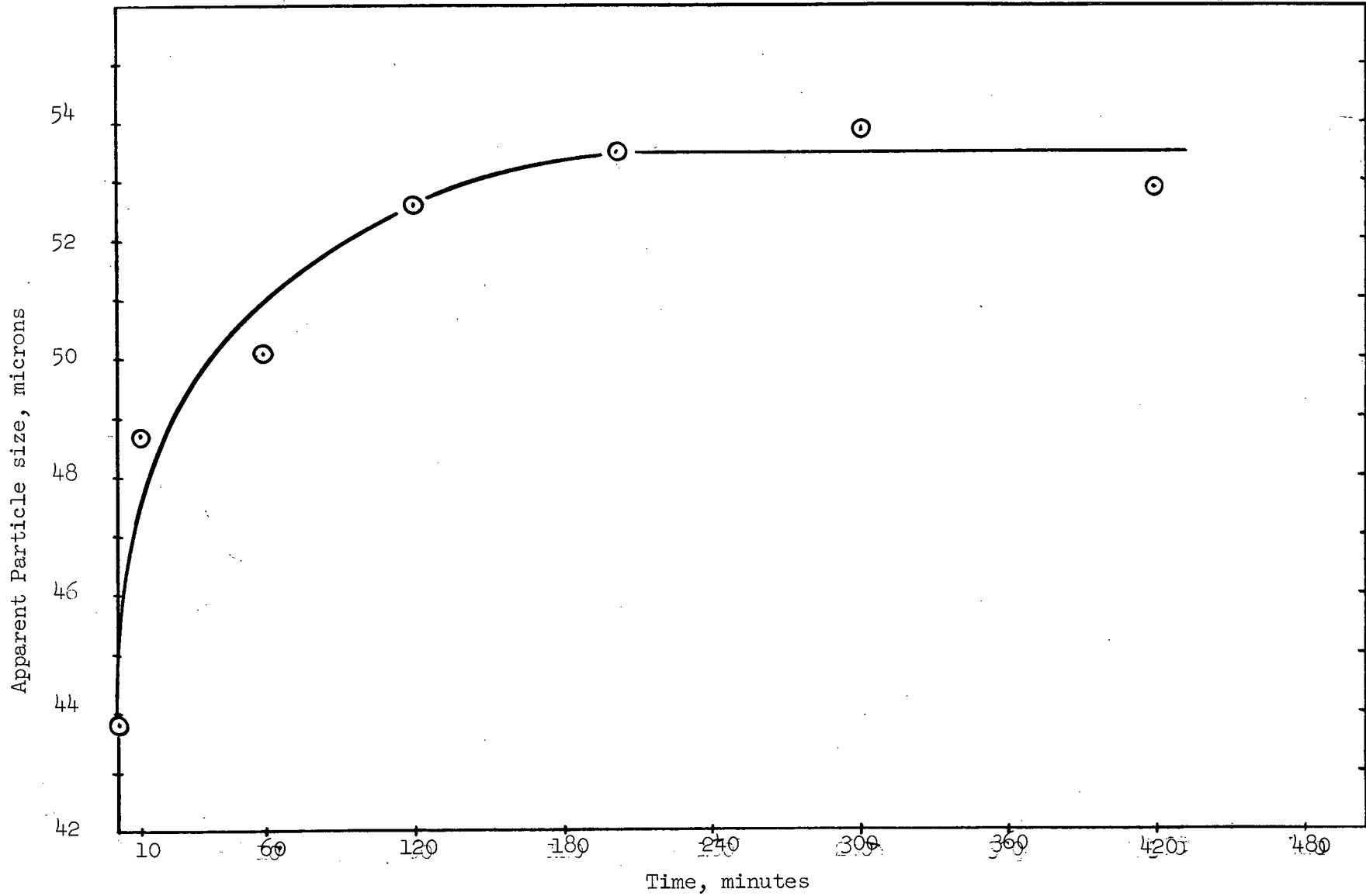


Figure 2. Effect of Infiltration Time on Iron-Particle Size (apparent)
(Inf. Temp. 1150°C)

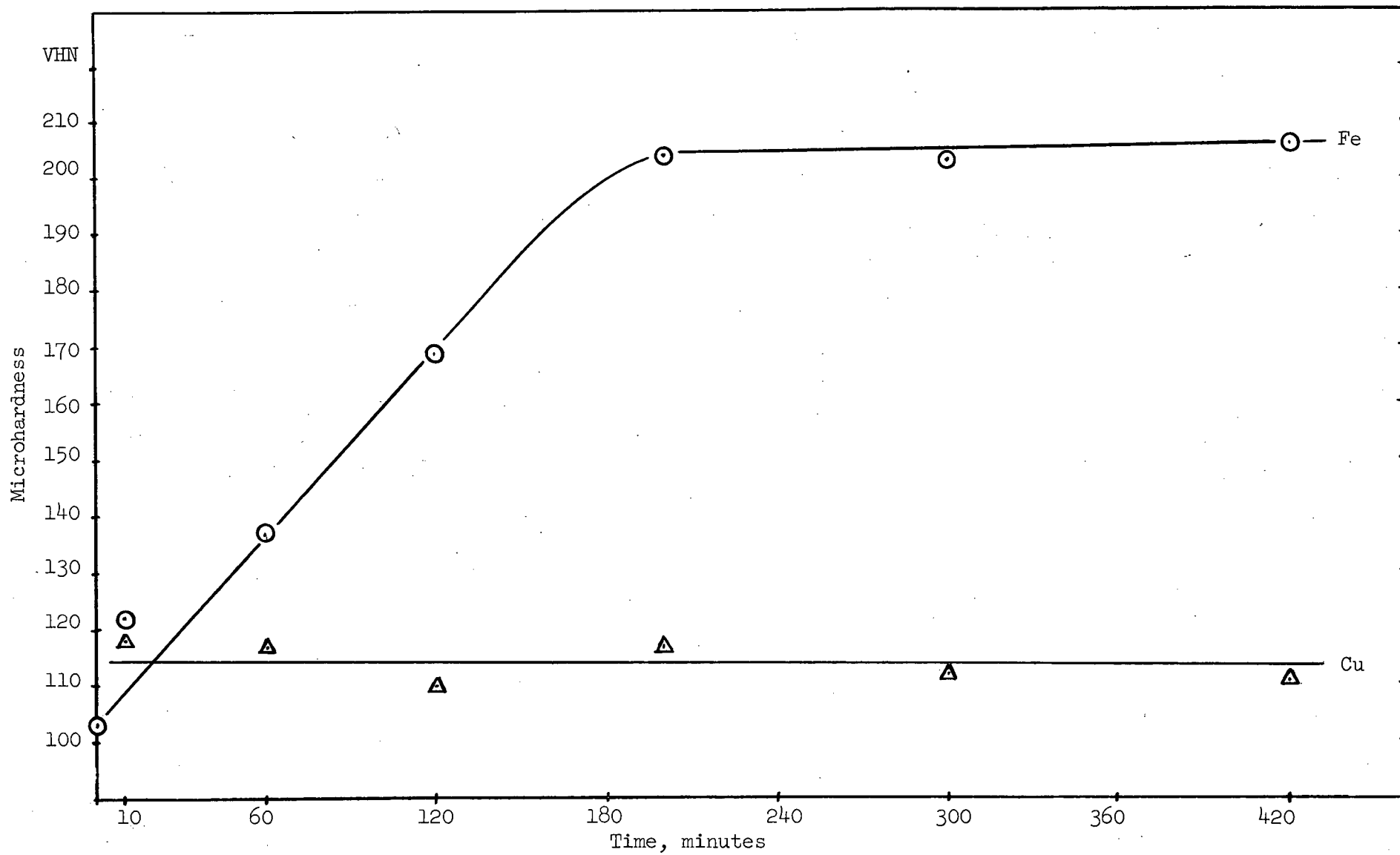


Figure 3. Effect of Infiltration Time on Microhardness of the Two Constituents (Inf. Temp. 1150°C).

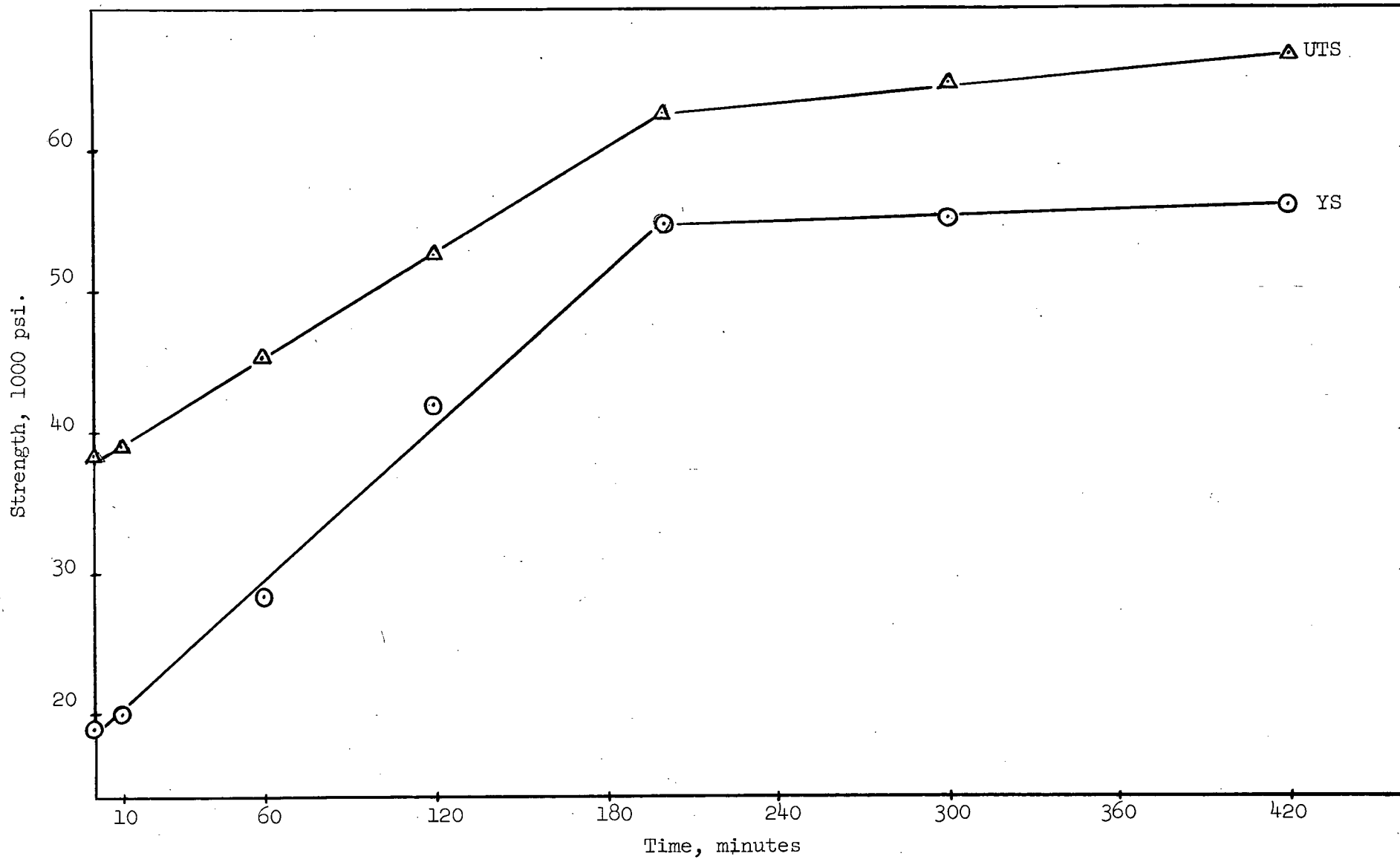


Figure 4. Effect of Infiltration Time on Strength of Copper Infiltrated Iron (Inf. Temp. 1150°C).

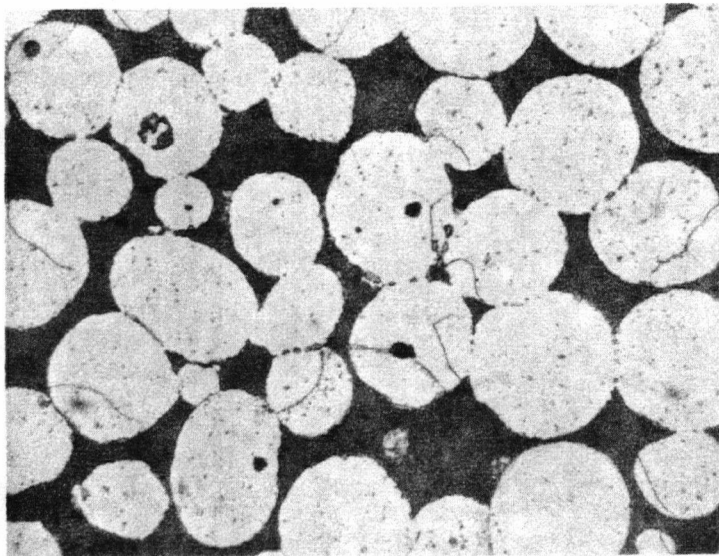


Figure 5. Sintered Iron Skeleton, 300 x.

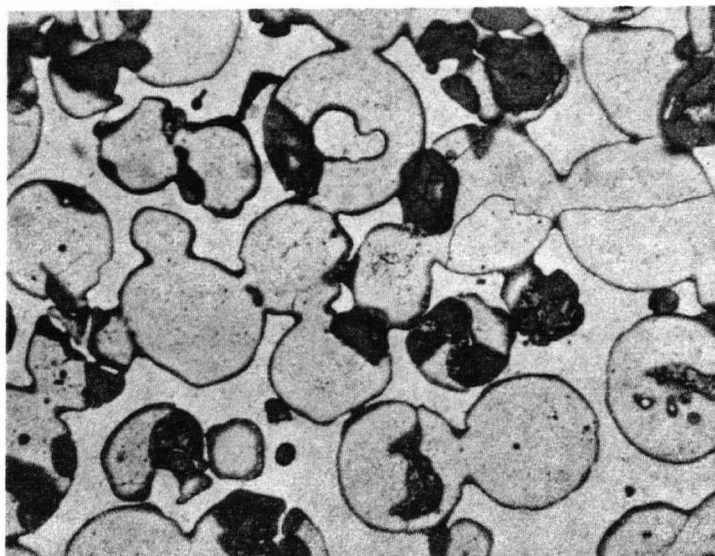


Figure 6. Specimen Infiltrated 10 min. at 1150°C,
300 x.

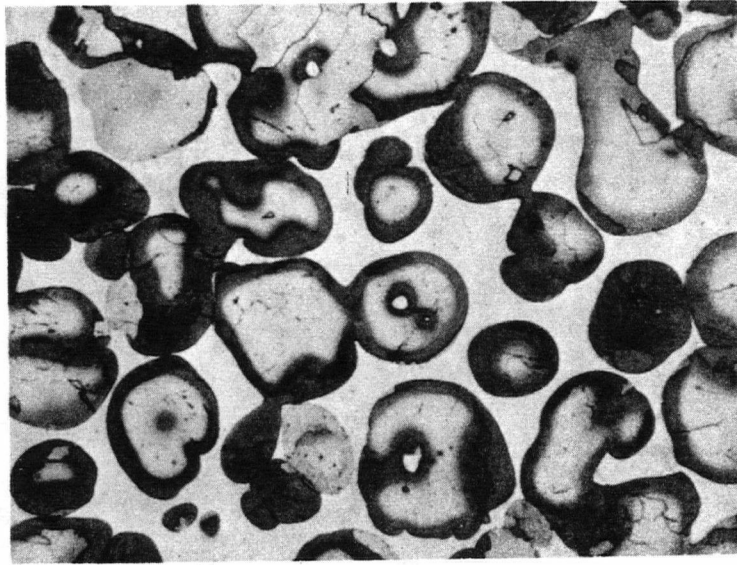


Figure 7. Specimen Infiltrated 120 min. at 1150°C.,
300 x.

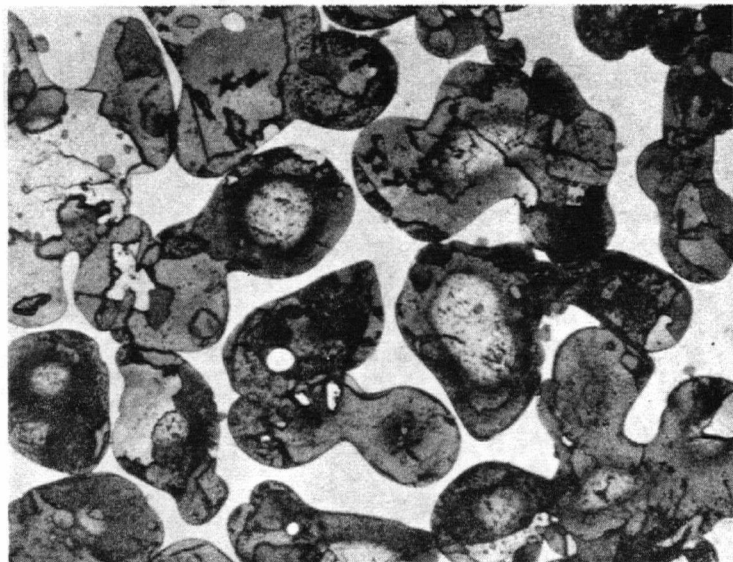


Figure 8. Specimen Infiltrated 420 min. at 1150°C,
300 x.

- f. Both yield and tensile strengths (Figure 4) increases linearly with time up to 3 hours of infiltration after which the rates of increase drop to considerably lower values.
- g. The ductility measured as elongation to fracture decreases with increasing time of infiltration.

Micrographs of a sintered iron skeleton and of specimens infiltrated for 10, 120 and 420 minutes are given in Figures 5, 6, 7 and 8 respectively.

2. Infiltration Temperature

Specimens similar to the ones used in the previous time series were infiltrated for 10 minutes at 1100, 1150, 1260 and 1370°C. The properties obtained are presented in Table 2 and in Figures 9, 10, and 11. Additional tensile data are contained in Appendix II.

The observations are basically the same as in the time series. The infiltrated density, (except at the lowest temperature), the volume ratio of the constituents and the hardness of the Cu-rich matrix were independent of the infiltration temperature, whereas the iron-particle size, the mean free path, the hardness of the Fe-rich constituent and the ultimate and yield strengths increased as the infiltration temperature was increased. Ductility decreased with increasing temperature. However, no leveling off of any of these parameters was observed within the temperature range investigated.

It was also observed that specimens infiltrated at 1100°C showed a considerably larger amount of grain boundary penetration than the ones infiltrated at higher temperatures (see Figure 12). At temperatures close to the melting point the surface tension of liquid is relatively high and the molten copper layer formed around each Fe-particle exerts a significant compressive force, which effects the γ_{SS} of the iron and renders grain boundary penetration more favorable.

TABLE 2

Infiltration Temperature (10 min)
200 x 270 Iron Powder

Temp °C.	Start. Dens. %	Inf. Dens. %	Cu content		Ratio Met/ Calc.	Fe Part Size		Ratio Met/ Sieve	Int. Part. Space μ	Mean Free Path μ	Hardness ^{AA}		YS psi.	UTS psi.	E %	Spec No.
			Calc. %	Met. %		Sieve μ	Met. μ				Fe VHN	Cu VHN				
-	70.7	-	-	74.6	1.05	63	43.8	0.70	58.7	14.9	103	-	19000 ^{AAA}	38500 ^{AAA}	45.0 ^{AAA}	40
1100	78.3	96.8	21.7	23.5	1.08	63	46.7	0.74	61.0	14.3	118	110	18800	37000	13.5	46
1150	77.7	98.0	22.3	19.6	0.88	63	48.7	0.77	60.5	11.8	122	118	20000	39100	9.4	28
1260	77.2	98.3	22.8	19.7	0.86	63	51.3	0.81	63.9	12.6	140	118	36700	52400	8.0	44
1370	76.9	97.8	23.1	20.9	0.91	63	50.1	0.80	63.3	13.2	165	111	53200	60800	2.0	78

^{AA} 50 g load

^{AAA} A.S.M. Metals Handbook 1948, p. 432

Abbreviations - See Table 1

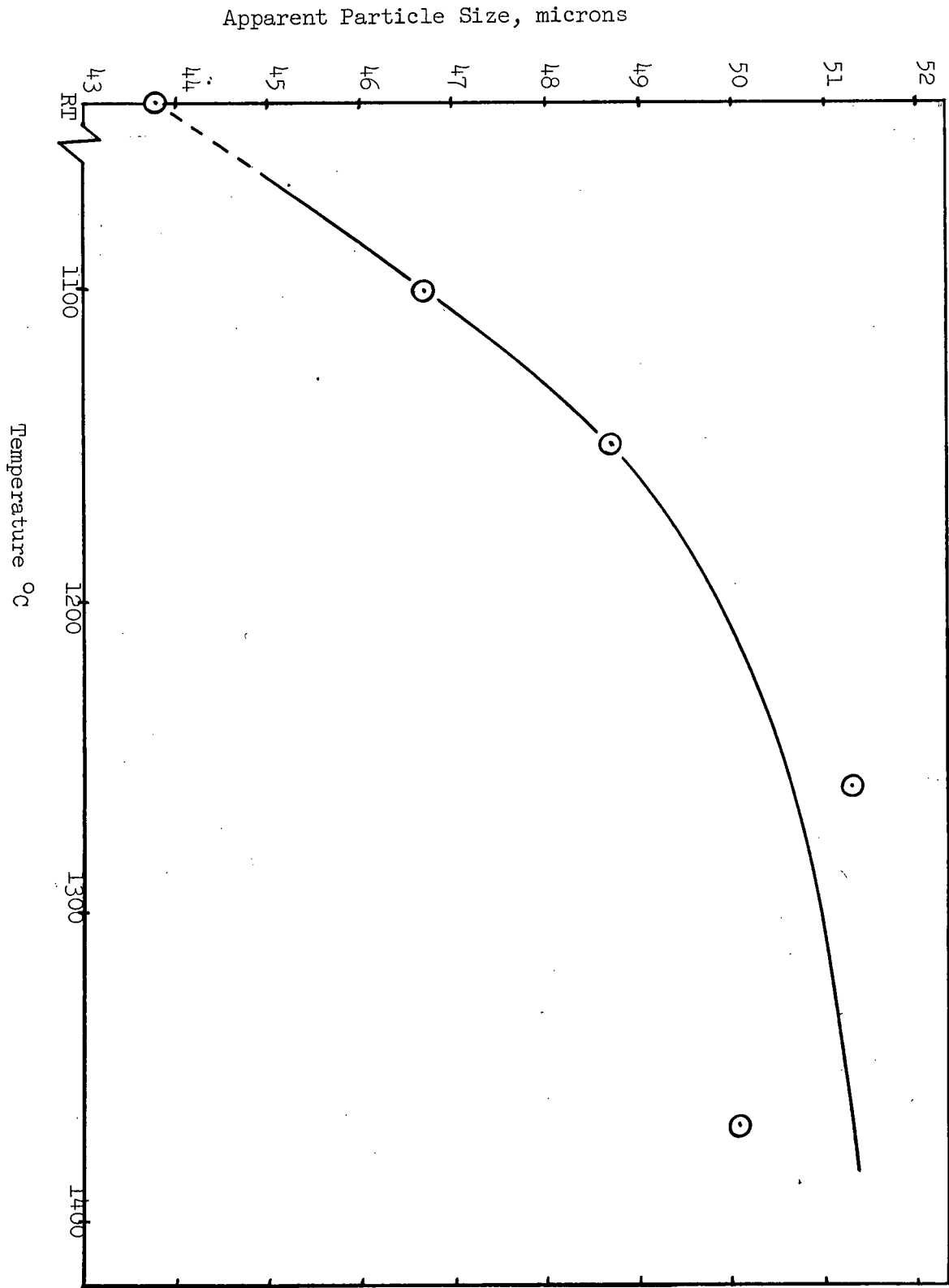


Figure 9. Effect of Infiltration Temperature on Iron-Particle Size (Apparent)
 (Inf. Time 10 min.)

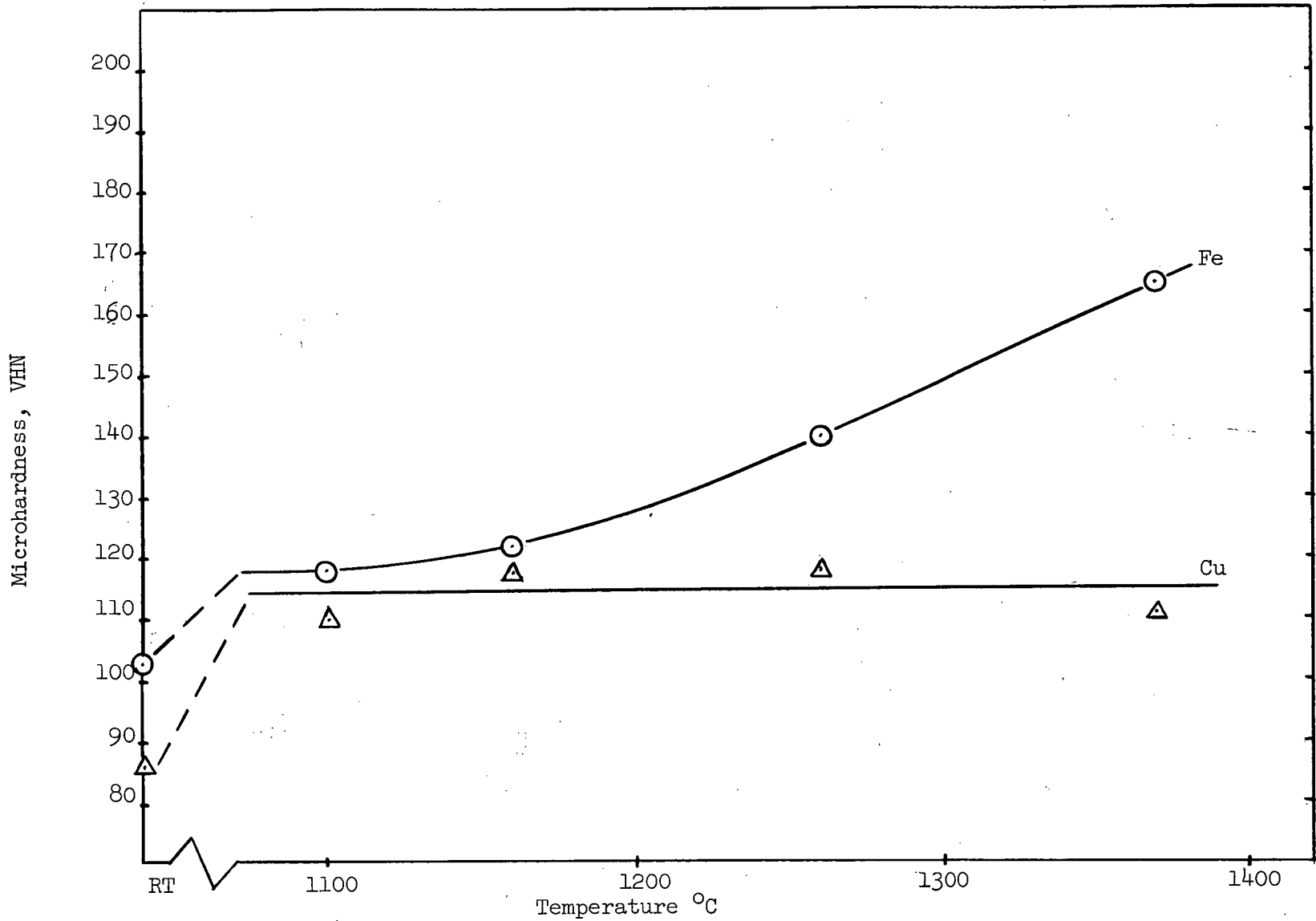


Figure 10. Effect of Infiltration Temperature on Microhardness of the Two Constituents (Inf. Time 10 min.).

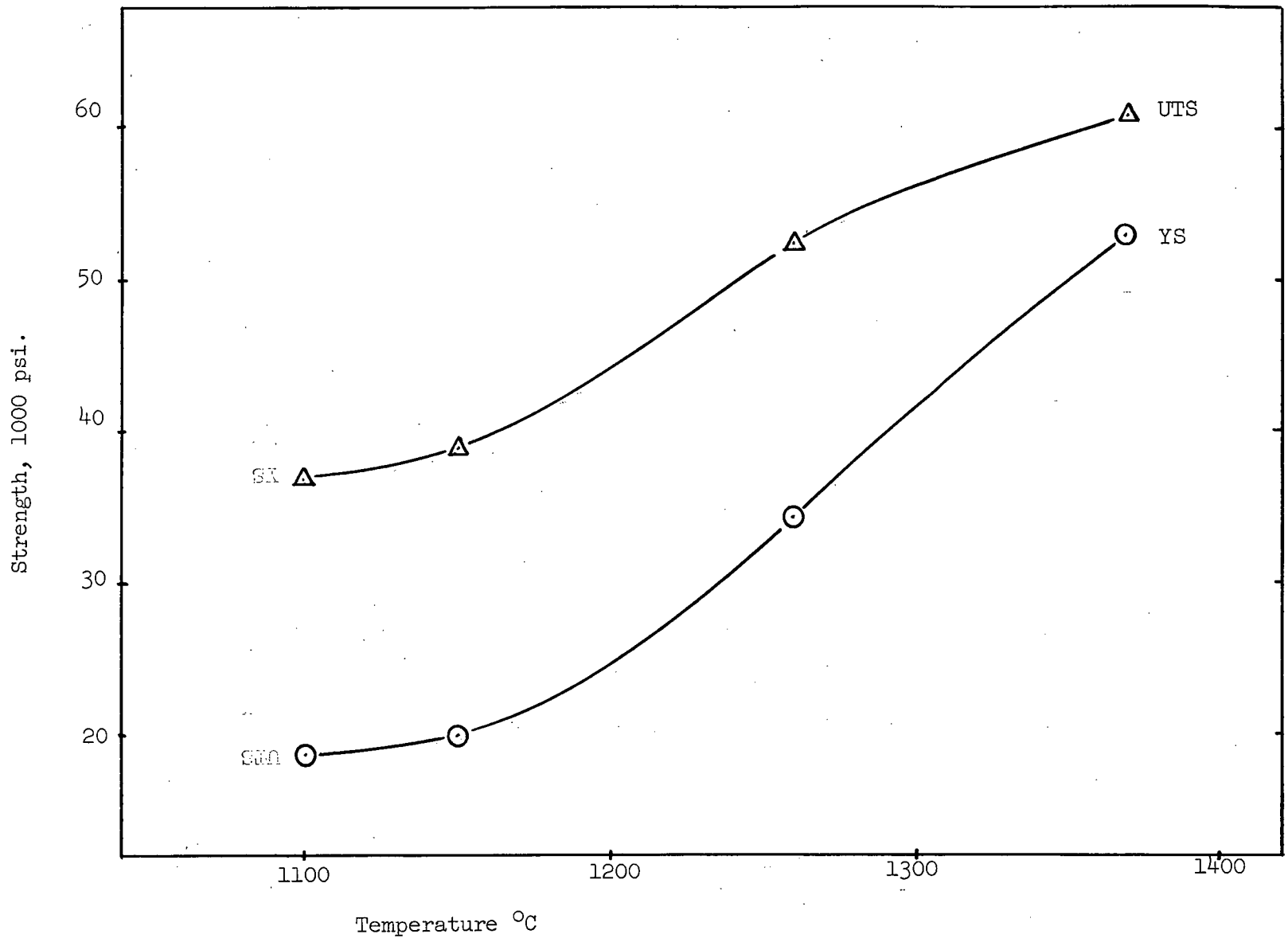


Figure 11. Effect of Infiltration Temperature on Strength of Copper Infiltrated Iron (Inf. Time 10 min.)

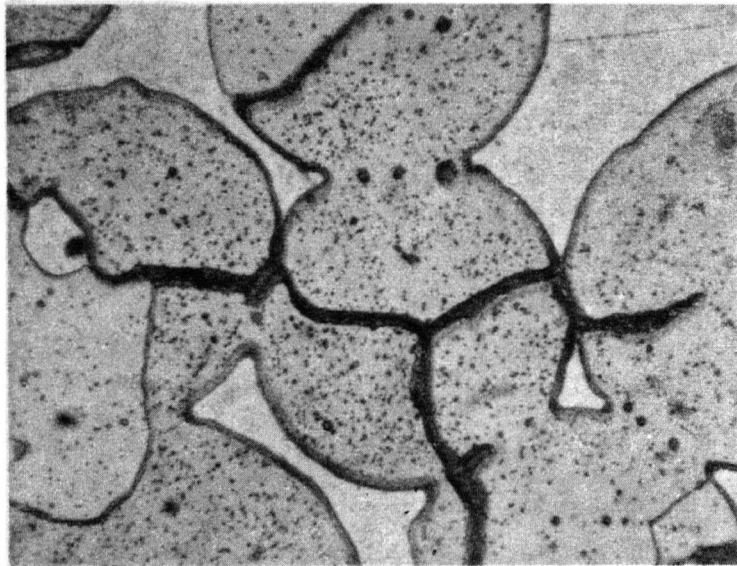


Figure 12. Grain Boundary Penetration of Cu into Fe, 800 x.

3. Volume Fraction of Infiltrant.

Specimens were made from 200 x 270 mesh iron powder at zero, 20,000 and 30,000 psi. compacting pressure followed by sintering. One of two groups compacted at each pressure was infiltrated for 10 minutes at 1150°C, the other group for 120 minutes at 1150°C. The infiltrated properties and other relevant data are given in Table 3. Reproducibility tests are contained in Appendix II.

Examination of these results show that:

1. The amount of final infiltrated porosity does not depend on the ratio of the volumes of the two constituents in the range of 18 to 40% copper.
2. The apparent iron-particle size after infiltration increases with an increasing amount of iron in the initial compact.
3. The matrix mean free path increases linearly with the volume fraction of copper and this relationship is not affected by the infiltration time (Figure 13).
4. The microhardness of the iron constituent, and the yield strength, tensile strength and elongation of the composite are influenced by the time of infiltration (as noted previously) but are independent of the volume ratio of the two constituents and of the mean free path between the hard (iron rich) regions.

TABLE 3

Volume Fraction of Infiltrant (Inf. at 1150°C)
200 x 270 Iron Powder

	Start Dens. %	Inf. Dens. %	Cu content		Ratio Met/ Calc.	Part Size ^{Fe}		Ratio Met/ Sieve	Int. Part. Space μ	Mean Free Path μ	Hardness ^A		YS psi.	UTS psi.	E %	Spec. No.
			Calc. %	Met. %		Sieve μ	Met. μ				Fe VHN	Cu VHN				
Inf.	63.3	98.0	36.7	39.9	1.08	63	43.2	0.69	71.9	28.7	145	106	23,200	43,200 37,300	7.5	36
10 min.	69.8	97.3	30.2	27.7	0.92	63	47.9	0.76	66.4	18.5	148	105	23,000	32,400	3.5	39
min.	77.7	98.0	22.3	19.6	0.88	63	48.7	0.77	60.5	11.8	143	126	20,000	39,100	9.4	28
Inf.	60.2	98.4	39.8	37.7	0.95	63	44.7	0.71	72.0	27.3	172	106	35,200	42,200	4.0	61 b
120 min.	71.4	98.1	28.6	26.0	0.91	63	46.3	0.74	62.5	16.2	193	111	45,600	50,700	2.0	66 b
min.	77.3	97.8	22.7	19.9	0.88	63	52.6	0.83	65.7	13.1	201	115	42,000	52,800	5.0	67

^A 10 g load

Abbreviations - see Table 1

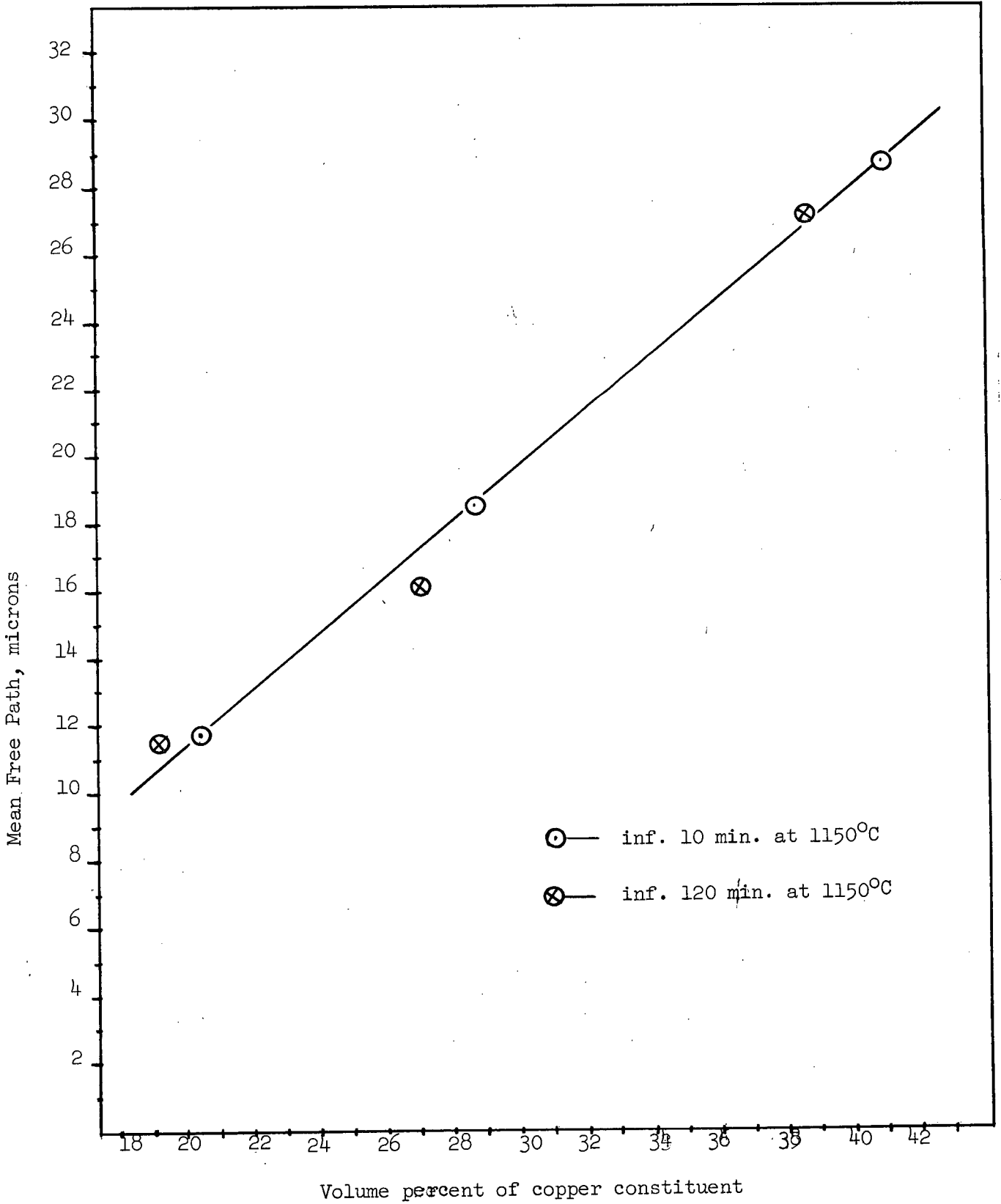


Figure 13. Mean Free Path versus Volume Percent. of the Copper-Rich Constituent.

4. Particle Size of Iron

Two groups of specimens were prepared (using 30,000 psi. compacting pressure) from each of the five sieve fractions of iron powder. One set of specimens was infiltrated for 10 minutes, the other for 120 minutes, at 1150°C.

The results of testing these specimens are collected in Table 4. Additional tensile test data appears in Appendix II.

The following observations can be made:

1. Iron-particle growth (as a percentage increase) is more pronounced for the finer particles and longer times.
2. The matrix MFP increases linearly with increasing iron-particle size for both infiltration times (Figure 14).
3. The microhardness of the matrix shows a tendency to increase with a decrease in the iron-particle size.
4. The hardness of the iron-rich constituent did not change with the particle size in the case of 10 min. infiltration, but increased considerably with decreasing particle size with the longer infiltration time.
5. No consistent variation with particle size was found in the case of yield and tensile strengths.
6. High ductilities, up to 25% (see Appendix II) were observed for the coarser powder fractions with short infiltration time, and this ductility decreased rapidly with decreasing particle size (Figure 15). The specimens infiltrated for 120 min. all had low ductility.

TABLE 4

Particle Size
(Infiltrated at 1150°C)

	Sieve Fraction mesh	Start. Dens. %	Inf. Dens. %	Cu content		Ratio Met./Calc.	F ₈ Part. Size		Ratio Met./Sieve	Int. Part. Space	Mean Free Path	Hardness [*]		YS psi.	UTS psi.	E %	Spec. No.
				Calc. %	Met. %		Sieve	Met.				Fe VHN	Cu VHN				
Inf. 10 Min.	-100 +150	75.8	96.9	24.2	22.3	0.92	127	81.0	0.64	104.2	23.2	148	92	20,900	41,300	20.0	50
	-150 +200	77.3	97.7	22.7	23.2	1.02	89	58.8	0.66	76.5	17.7	143	106	23,200	41,300	17.5	53
	-200 +270	77.7	98.0	22.3	19.6	0.88	63	48.7	0.77	60.5	11.8	149	126	20,000	39,100	9.4	28
	-270 +325	75.4	97.5	24.6	24.0	0.94	48	37.9	0.79	49.8	11.9	153	111	23,600	46,600	12.0	55
	-325	74.0	97.5	26.0	21.5	0.83	25	21.7	0.87	27.7	6.0	154	117	27,500	37,400	5.0	57
Inf. 120 Min.	-100 +150	74.0	98.2	26.0	24.5	0.94	127	92.7	0.73	122.5	30.2	140	95	36,400	53,500	7.5	73
	-200 +270	77.3	97.8	22.7	18.2	0.80	63	51.7	0.82	63.3	11.6	201	115	42,000	52,800	5.0	67
	-270 +325	76.2	97.9	23.8	25.3	1.06	48	40.9	0.85	54.7	13.8	197	105	41,100	41,300	0.5	85
	-325	79.8	99.2	20.2	21.5	1.06	25	34.3	1.37	43.6	9.3	229	125	40,200	40,400	0.5	86

* 10 g load

Abbreviations - see Table 1

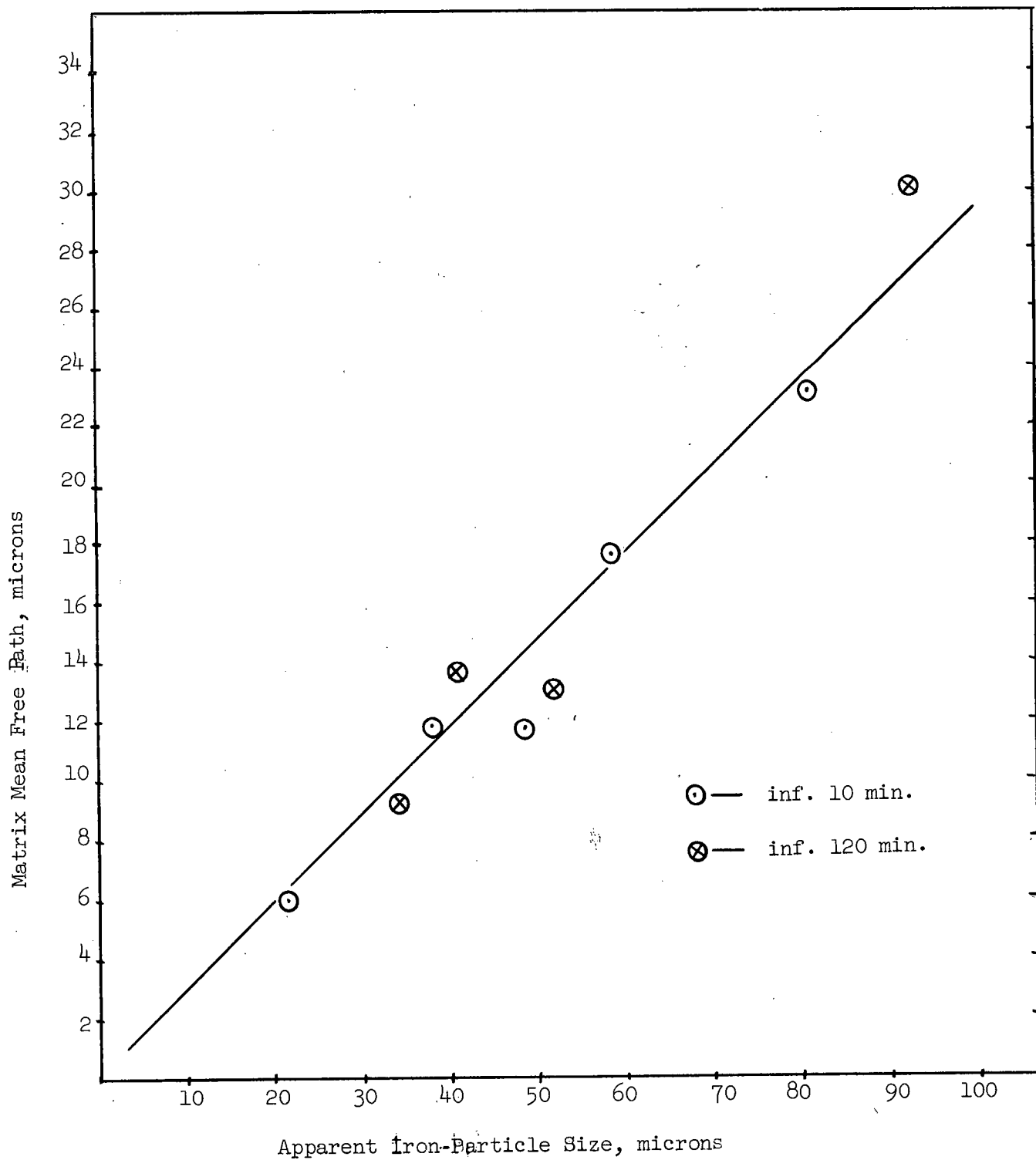


Figure 14. Mean Free Path versus Iron-Particle Size (apparent)

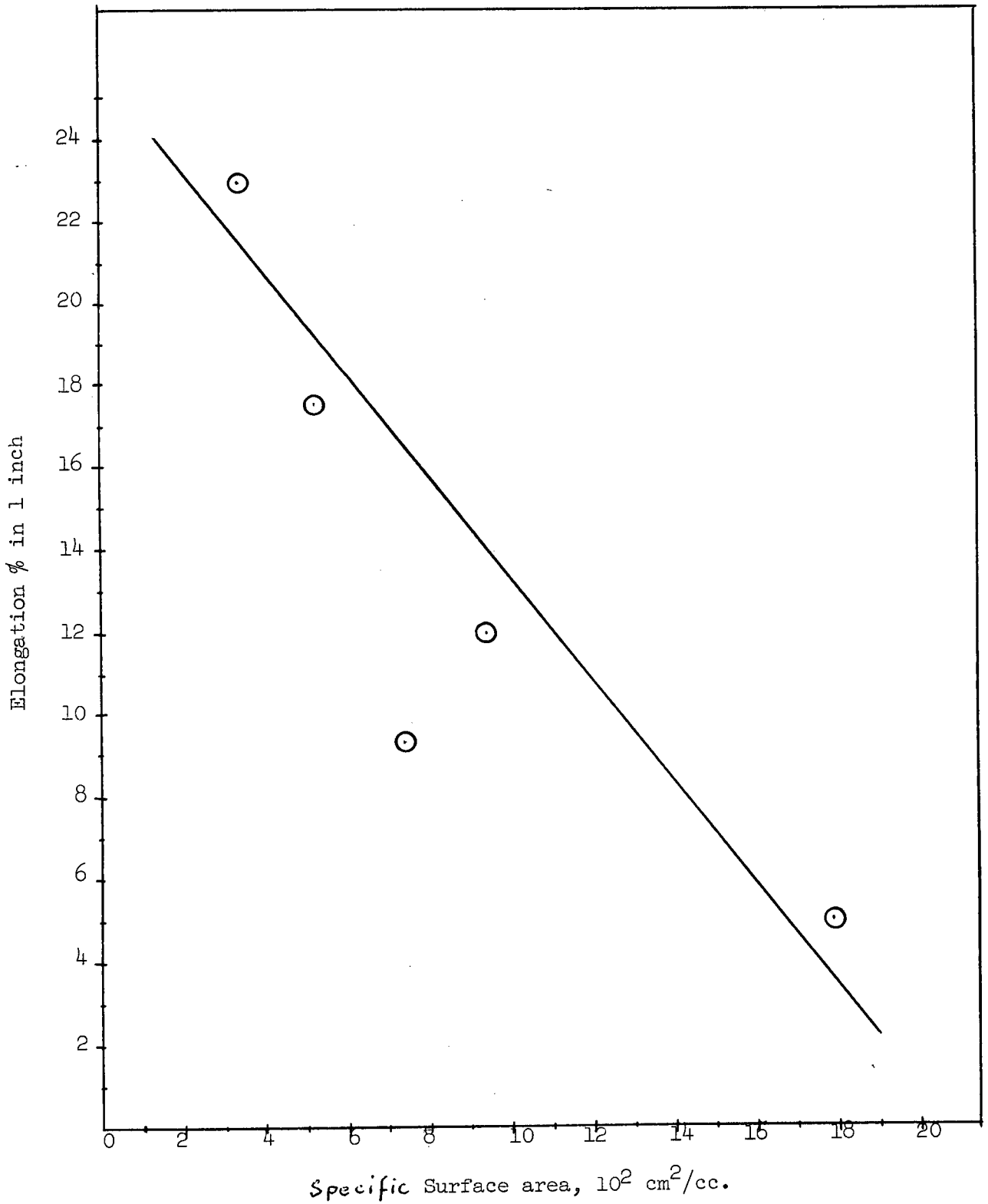


Figure 15. Elongation versus Surface Area of Iron-Rich Particles (10 min. Infiltration at 1150°C)

Additional Experimental Results

a. Constitution

The constitution of each specimen was calculated based on the assumption that the relationship $(\text{Fe/pores})_{\text{sint.}} = (\text{Fe/Cu})_{\text{infilt.}}$ holds. The comparison of densities calculated on this basis with the ones measured metallographically indicated that the latter, on the average of 22 samples, gave 4% higher values; i.e. 1% higher in absolute copper content by weight.

In three cases the composition was analyzed chemically.

No. of spec.	Vol.%Fe	Cal.Vol.%Cu (pores deducted)	Calc. w.% Cu adjusted for 4% dissolv. Fe	Analyzed W.% Cu (wet)
45	78.0	19.6	21.3	22.7
28	77.7	20.3	22.2	26.0
37	62.6	35.1	38.2	40.7

The higher copper contents obtained by chemical analysis are expected since the other two methods give only the volume percent of the matrix copper whereas the wet analysis includes that copper which is dissolved in the iron-rich constituent.

b. Lattice Parameter of the Iron-Rich Constituent

X-ray diffraction using $\text{FeK}\alpha$ radiation was carried out on powder obtained from specimen No. 25 (inf. 200 min. at 1150°C). The Debye-Scherrer pattern revealed complete sets of BCC and FCC lines. The lattice parameter of the iron-rich phase calculated from the BCC lines was found to be $a = 2.8668 \text{ \AA}$. The reported value² for $\text{Fe}(\alpha)$ is $a = 2.8606 \text{ \AA}$; hence, $\Delta a = 0.22\%$ due to the solution of copper in iron.

c. Cooling Rate Effects

Specimen No. 58 (inf. 420 min. at 1150°C) was subjected to cooling rate studies. One section was tested as-infiltrated; i.e. the hot specimen (1150°C) was pulled into the cold part of the quartz tube and allowed to cool while the tube was sprayed externally with water.

The other two sections were annealed in cracked ammonia for 1 hour at 1000°C in a tube furnace. One was water quenched from this temperature, the other was furnace cooled. The mechanical properties were found to be as follows:

<u>Cooling Rate</u>	<u>YS psi.</u>	<u>UTS psi.</u>
water quench	48,000	59,600
process cool	46,300	49,200
furnace cool	28,700	39,700

As expected, the cooling rate affects the mechanical properties. However, this effect is not large in the range of high cooling rates. In particular, the yield strengths of the water quenched and process cooled specimens are very similar. Therefore it can be assumed that the properties obtained in the present experiments are not appreciably affected by minor changes in cooling rates from specimen to specimen (speed of withdrawal, weight of specimen, etc.).

d. Properties of Bulk Copper-Rich Alloy

For reference data an iron-saturated copper alloy specimen was prepared and tested. Twenty-five grams of copper and 1 gram of Atmco iron powder were placed in a hydrogen cleaned thin-walled mild steel tube of I.D. 0.360", welded closed at one end. After evacuation with a fore-pump the tube was placed vertically into the furnace for 1/2 hour at 1150°C. During this time the copper became saturated with iron. After this the tube and contents were water quenched and swaged in two passes for a total reduction of area of 61%. This was followed by

annealing for 10 min. at 1050°C. in vacuum, and a water quench. The properties obtained on machined tensile specimens were:

VHN	YS	UTS	E
86	24,400	47,200	30

e. Relative Plastic Deformation of the Two Constituents

Specimens No. 19 and No. 46, which showed considerable plastic deformation prior to failure (25% and 13.5% elongation respectively) were examined metallographically to obtain the relative deformation of the two constituents.

The iron-rich particles in an undeformed specimen are spherical. During tensile deformation they become elongated along the specimen axis. If both phases deform the same amount, i.e. the interface is coherent during deformation, the shape change of any iron particle should follow the deformation of the whole specimen.

In order to verify this, in the longitudinal metallographic section of each specimen 12 particles were measured for their longer and shorter axes, a and b. These particles were chosen in the uniform deformation zone at about 1/4" distance from the fracture. On the average of 12 measurements the following data were obtained.

Spec. No.	a	b	a/b	calc. a/b
19	170	121	1.41	1.40
46	98	80	1.225	1.21

The calculation of a/b was based on an ellipsoidal shape of the deformed iron particles.

$$\text{Volume} = \frac{4}{3} \pi ab^2 = \frac{4}{3} \pi r^3$$

where a = 1.25 r for specimen No. 19
 a = 1.135 r for specimen No. 46

The measured iron-particle elongation determined in this manner after fracture agreed within 1% strain with the total elongation of the composite.

f. Effect of Gas Pressure in Infiltration

During infiltration of specimen No. 62c (2 hrs. at 1150°C) after the 10th and 60th minute the vacuum line was closed off and argon was let into the infiltrating tube at a pressure slightly above atmospheric. The overpressure was maintained for 2 minutes, after which the vacuum was re-established. The final composite density, 98.25%, was apparently not affected by this treatment.

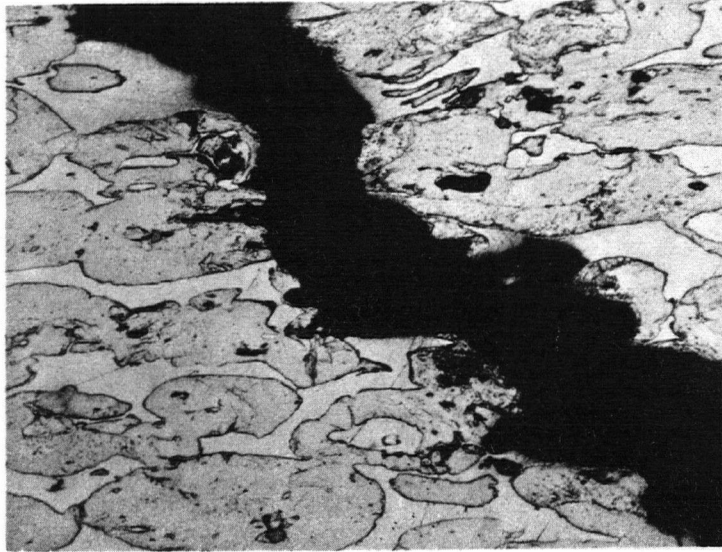


Figure 16. Fracture after Large Plastic Deformation, 150 x

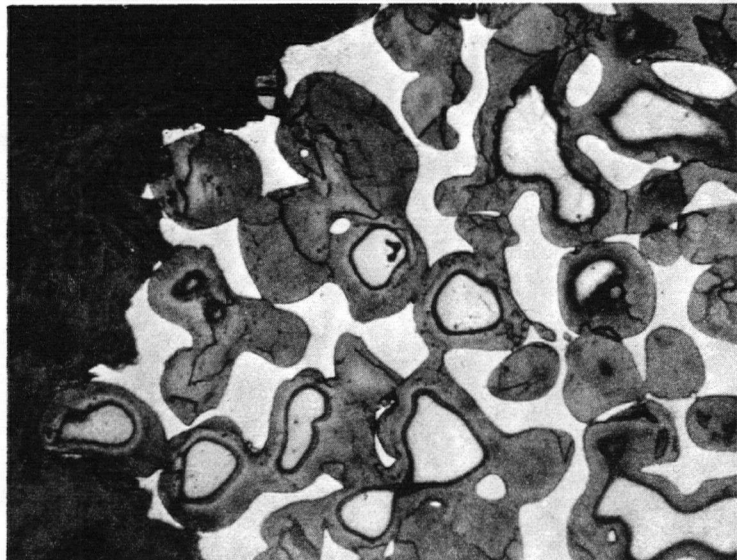


Figure 17. Brittle Fracture, 300 x.

IV. DISCUSSION

1. Porosity in Composites

Residual porosity was found in the microstructures of all infiltrated samples. Similar observations were made by Elliot¹, while Frantzevich¹⁷ and Semlak³⁰ reportedly obtained dense specimens after 2 - 5 minutes and 30 minutes of infiltration respectively.

The amount of porosity in the present study was quite constant ($1.8 \pm 0.4\%$) for the majority of the specimens infiltrated under various conditions, with the notable exception of specimens infiltrated at a temperature just above the melting point of copper. The latter specimens were less dense than the others ($\sim 3.5\%$ porosity).

The most obvious explanation for porosity is that it originates from entrapped gases. However, infiltration was carried out in vacuum. Other facts are also against the possibility that gases desorbed from Fe particles by the moving copper phase would collect or reabsorb in the pores.

In the present infiltration procedure the infiltrant probably does not enter the skeleton from the bottom upward but rather rapidly from the sides toward the specimen axis. This assumption is based on the poor heat conductivity of the cold compact which allows the outside surfaces to heat above the melting point of copper considerably faster than the centre. This sequence of infiltration would be expected to trap gases at the centre of the specimen. However, the distribution of the pores was found metallographically to be completely random radially or along the specimen axis. The pore size varied from 2 to 10 μ .

The amount of porosity was not affected by the time of infiltration between 10 and 420 minutes, which further weakens the argument for entrapped gases. More doubts arise from the fact that a cyclic variation of external pressure during infiltration had no effect on the final density.

The possibility that the pores result primarily from the shrinkage of copper upon freezing has also been considered. The density ratio for copper $\frac{\rho_L}{\rho_s} = 4.92\%$. Thus with 25% of copper the shrinkage would account for 1.2% porosity, which is of the right magnitude. However, since the same porosity was observed for 37% as for 23% copper this argument is not wholly satisfactory either.

Although the origin of residual porosity is not clear, its effect on the properties of infiltrated material is pronounced. The distribution of pores is essentially random but the statistical probability of having a certain critical number of pores in one plane could lead to high stress concentrations, crack nucleation and premature failure of the specimen.

Actually this is believed to be the case with a large number of specimens, particularly those with a hard iron-rich constituent, where the hydrostatic stress in the matrix is high and thus any stress-raising effect is more significant. On the basis of the reproducibility of experiments it can be said to a high degree of certainty that yield strengths are very little affected by porosity, the UTS values are affected to a larger extent, and elongation values are strongly affected. Similar observations were made by Edelson and Baldwin⁹.

2. Growth of the Iron-Constituent Particles

Pronounced growth of some iron particles was observed in every set of experiments. In assessing this growth phenomenon reference should be made to section II-5 (b) of this thesis which discussed the effect of size distribution on the "apparent" particle size obtained metallographically.

Particle growth increased with time, with temperature, with fineness of the original iron particles, and with increase in the volume fraction of iron. (see Figures 2 and 9).

During the first stage of infiltration and liquid phase sintering of iron-copper, particle growth, sometimes very extensive, has been observed by many workers,^{1,3,19,31}. Rennhack²¹ reported that he observed the same phenomenon but only at a later stage, after complete saturation of iron with copper had occurred.

Price³², studying the W-NiFeW system, also observed extensive growth which he attributed to the preferential dissolution of smaller grains (less than 1μ), due to their greater chemical activity, and reprecipitation of this excess solute onto the larger particles. However, it is believed that in the present work such effects could not play an important role. The particles in these experiments were initially of narrow size distribution, were almost perfect spheres, and were relatively large.

Elliot¹ explained the growth by the expansion of iron due to copper entering solution and by the precipitation of excess iron from solution. However, calculations indicate that at full saturation (8% Cu in Fe by weight), in the case of 65μ diameter particles the linear size increase, Δd , would be $\sim 2\%$, while the observed maximum growth in the present work was 22%. This clearly suggests that some solution-reprecipitation process occurs, although the

driving force for this mechanism has not previously been explained.

Since particle growth in these experiments and in most other reported studies stopped at about the same time as the hardness increase, and since no growth was observed with presaturated particles¹ it is reasonable to assume that the growth is controlled by the diffusion of copper into iron, or by the degree of saturation of the iron with copper.

On the basis of this the following tentative mechanism is offered. Two stages of growth are considered corresponding to two largely different slopes in Figure 2. In the first stage, which is very rapid but does not account for a large volume fraction of the growth, copper penetrates into the iron through favorably oriented grain boundaries and as a consequence the grains are forced apart. As it was reported by Bredz³³, in very short times (2 min. at 1100°C) the amount of Cu which has penetrated the iron this way can be 5000 times larger than that which has diffused directly into the iron lattice.

The second and more important suggested stage of growth is an indirect result of lattice diffusion. It has been determined by Teodorovich²² using electron microscopy that during diffusion of Cu into Fe, a Kirkendall effect produces a high vacancy concentration at the interfaces. It is reasonable to expect that these defective regions have greater than normal apparent interfacial energy. Since the rate of diffusion of Cu into Fe (as the etching patterns indicate) varies from particle to particle and even within one particle, the apparent interfacial energy must be assumed to vary also from one particle to another. This interface energy difference would result in a flux of iron toward the defect surfaces in order to reduce their excess energies. This process is in operation only as long as the diffusion rate of copper in the iron is significant.

In the case of specimens with high volume fraction of copper, the lower growth rate is probably due to the larger interparticle spacing.

3. Effect of Various Factors on the Tensile Properties of Composites.

a. Matrix Mean Free Path (MFP) and Interparticle Spacing of the Iron (IPS)

In the present work the MFP was controlled by changing the volume fraction of the matrix and the particle size of the iron. By these methods a MFP range of 6 to 29 μ was obtained.

Examination of the data given in Table 3 and 4 and Appendix II indicates that the change of MFP had no significant effect on the yield strength, tensile strength or elongation.

In those series of tests in which major changes occurred in composite properties (e.g. in the time and temperature series, Tables 1 and 2) the MFP was essentially constant.

The IPS is the average distance between the centres of two adjacent iron-rich particles. For relatively large particles, such as those used in the present experiments, the IPS is made up of three components, the radii of each of two particles, and the shortest distance between their surfaces. This latter dimension is proportional to the mean free path, the effect of which was discussed in the previous section. The sum of the two radii gives the mean particle size, which was varied during the experiments by using powders of various sieve fractions while the volume ratio of the two phases was kept constant. Consequently, a decrease in particle size also meant a decrease in mean free path. The relationship between these two parameters is linear (Figure 14).

The variation of particle size was about 4 fold, from 22 μ to 81 μ diameter, which is equivalent to a 14 fold increase in surface area and a 50 fold increase in the volume of individual particles per unit weight. This had no apparent effect on the YS and UTS values, the changes of which were in no way consistent with the particle-size changes (Table 4).

The elongation values, however, showed a well-defined trend at least in the short infiltration time series. With a decrease of the particle size, the elongation decreased from 20 to 5%.

In spite of the lack of confidence which is placed in absolute elongation measurements, this fact is interesting since in these tests the \bar{V}_S and UTS remained practically constant. It is possible that, if the work hardening rate is low, large changes in ductility are accompanied by small changes in UTS.

Krock¹⁰ has suggested that the surface or interface condition of the hard phase has a very critical effect on ductility.

As has been already mentioned the surface of the iron particles was found by Teodorovich²² to contain a large excess concentration of vacancies. In the experiment under discussion, because of the short infiltration time involved (10 min.) a unit area of interface for any size of particle should contain approximately the same amount of defects. If this is so, and if the ductility is determined by conditions at the interface, there should be a relationship between the amount of interface in a given specimen and its ductility. A plot of these two parameters (Figure 15) gives a good indication of the existence of this predicted relationship, in view of the aforementioned experimental limitations.

b. Volume Fraction of Constituents

In the present experiments the volume fraction of the iron constituent was varied from 60 to 78%. The test results reported in Table 3 indicate that the yield strength and elongation were not affected by the ratio of the two phases in this range although there is not sufficient data to permit firm conclusions to be drawn.

Attempts were made to correlate the UTS data with values calculated from Pine's equation:

$$P = P_{Fe}x^2 + P_{Cu}(1-x)^2 + P_{FeCu}x(1-x)$$

However, neither the strength of the iron-rich phase, P_{Fe} , which changes with time according to the microhardness readings, nor the strength of the iron/copper interface, P_{FeCu} , are known from direct measurements. Strength values calculated by using $P_{FeCu} = 66,000$ psi as employed by Pines for the low-carbon iron/copper interface in his calculations, and P_{Fe} obtained from hardness-strength conversion charts for the given microhardness of the iron phase, were about 8,000-12,000 psi higher than the experimental strengths. However, the slopes of plots of strength versus the square of the volume fraction were not far from the calculated slopes. This indicates clearly that the volume fraction of the harder phase has some effect on the composite tensile strength, even though it is much less marked than the effect of infiltration time.

c. Hardness of the Iron Constituent

In the present studies each series of experiments gave clear evidence of the solution hardening which accompanied infiltration. The most direct evidence was the microhardness of the iron-rich constituent.

In the infiltration time series of tests the average microhardness of the iron increased almost linearly up to 300 minutes where it leveled off (Figure 3). But the microstructure provided definite evidence that the iron particles were not completely saturated with ^{copper}~~iron~~. The diffusion layer color was of decreasing intensity toward the centre of each particle (Figure 7!).

After the longest infiltration time studied, 120 minutes, the picture was similar but with less contrast. The obvious diffusion layers had moved somewhat deeper into the particles, Figure 8, the hardness difference had been slightly reduced. Though saturation of iron with copper was probably incomplete, the depth of penetration had reached an equilibrium value for the infiltration time employed.

The cause of the apparently sudden change of diffusion rate after 2 hours of infiltration is not clear. But the microhardness and the mechanical properties need not be expected to increase continuously to the point of complete saturation. Other workers report^{2,26} that the hardness and strength values of iron-copper alloys increase up to 2% copper only and that they level off beyond that concentration. The hardness values quoted for the 2% copper alloy are in fact comparable to those observed for the iron phase after 200 minutes infiltration.

Since the behavior of the yield and tensile strength curves (Figure 4) was essentially the same as that of the hardness of the iron-rich phase, it is reasonable to assume that the strength properties are solely controlled by the hardness of the iron phase or by the hardness difference between the two phases as suggested by Heheman³³.

In the present experiments the hardness of the matrix remained essentially constant, so that the hardness increase of the iron also corresponds to the increase of hardness difference.

The assumption that the composite strength is controlled by the stronger phase and not by the weaker is interesting. Comparing the numerical values in these experiments

	YS	UTS
matrix	24,400	47,200
composite	56,100	66,900

it can be seen that the strengthening due to the iron phase is considerable.

The mechanical properties reported for Amco iron and determined for the iron-saturated copper are very similar. This probably explains the observation that after short infiltration times both phases deformed similarly and failed after a relatively large amount of plastic flow (20-30%). The fracture path went through both phases with no apparent preference for either (Figure 16).

As diffusion progressed with increasing infiltration time, the iron lattice became more distorted (solution hardened), its strength increased and its ductility decreased. The high yield strength of the iron particles effectively increased the stress necessary for gross plastic flow in the matrix, and as a result high composite strength and low ductility were observed. The stress system in the matrix becomes essentially triaxial when a uniaxial load is applied to the specimen, and the situation became similar to that found in brazed joints. Bredas³³ reported that in Fe-Ag brazed joints the notch constraint factor (giving the ratio of the actual stress at which plastic deformation begins to the yield strength) could be as high as 4 for a certain thickness of the binder.

At a critical value of the applied stress, in the limiting case of an extremely hard second phase, the specimen fails in a brittle manner with the fracture going preferentially through the copper-rich phase or along the interface (Figure 17).

In the light of the solution hardening mechanism many observations made during the course of these experiments can be explained. Since diffusion depends on time, temperature and distance, it is obvious that longer times and higher temperatures of infiltration, as well as smaller particles, should give higher strength values, in good agreement with observations.

It is necessary to note that in the literature the reported values of the strength of copper infiltrated iron are in some cases substantially higher than those obtained in the present experiments. This is most likely due to differences in the purity of the iron used. Schwartzkopf²⁴ found that the addition of 0.25% graphite to Fe prior to infiltration increased the composite yield strength from 61,000 to 72,900 psi. and the ultimate tensile strength from 67,500 to 76,100 psi. The iron used in the present work was of high purity relative to the carbonyl and other iron powders used in much reported experimental work.

4. Summary

In evaluating the deformation behaviour of copper-infiltrated iron compacts one has to bear in mind that few properties of metals are as sensitive to crystalline structure as those associated with yielding and flow. There seems to be little agreement in the literature about the precise dependence of deformation behaviour on the structure of a two-phase alloy. These systems are usually too complex, with too many variables involved, to lend themselves to mathematical calculations derived from simple models.

A dislocation theory approach to two phase systems by Lenel³⁴ predicts a relationship $YS = \sqrt{\mu b \mu' / 2 \lambda C}$ where μ and μ' are the shear moduli of the matrix and of the second phase particles respectively and λ is the mean free path. Empirical formulae which have been proposed^{8,11} also suggest that composite strength is proportional to the reciprocal of mean MFP. But the results of the present study indicate no dependence on MFP at all. One possible explanation for the apparently negligible contribution of MFP to the strength of these composites is the "masking" effect of other factors, like solution hardening of the copper-rich phase due to iron and the hydrostatic stresses in the matrix resulting from the different thermal expansion coefficients of the iron and copper-rich phases. The effect from MFP in the range studied contributes probably little to the residual stresses from the above mentioned two sources.

Edelson and Baldwin⁹ concluded that the presence of any second phase, if it is harder than the matrix, severely embrittles an alloy. The results of the present work are in disagreement with this conclusion. It seems that the role of the interface although secondary in yield strength considerations, is to reduce ductility through provision of stress raisers in the form of vacancy concentrations which arise through diffusion between the two components. This

implies that it is not the hardness of the second phase which determines ductility as proposed by Edelson but the degree of perfection of the interfaces and the degree of crystalline compatibility between the phases.

Finally it is interesting to note the many similarities between the Fe-Cu composites of this work and the W-NiFeW composites of Krock et al¹⁰. Both have high ductilities under certain conditions; their strengths are independent of MFP and volume fraction of the matrix and their strengths depend strongly on the relative hardness or strength of the second phase.

V. CONCLUSIONS

1. The major strengthening contribution in copper infiltrated iron composites is the hardness difference between the iron constituent and the copper-rich matrix. Any processing conditions which increase this difference increase the yield and flow strengths of the composite.
2. The tensile yield strength of the composite depends on the hardness of the iron-rich constituent only, and is apparently independent of the volume fraction of this constituent (in the range of 60-78%), the particle size, and the matrix mean free path between the particles.
3. The ultimate tensile strength is a function of the hardness of the iron-rich constituent but is apparently also a function of the volume fraction of this constituent.
4. The elongation to fracture depends on the hardness of the iron-rich constituent and on the area of the interface between the two phases.
5. The growth of iron particles which occurs during infiltration is the result of solution and reprecipitation of iron. The driving force for this process is believed to be a Kirkendall effect associated with the diffusion of copper into iron.

VI. APPENDIX I

Microhardness Testing

The use of microhardness testing in powder metallurgical practice where the microstructure is a complex mixture of different constituents of small dimensions involves a number of difficulties.

In order to measure the hardness of a given phase the impression must be small enough that the work hardened zone surrounding the impression does not reach the phase boundaries. But the small loads necessary for small indentations lead to relatively large errors. Buckler³⁵ has found the following relationship between load and relative error, arising from a constant error ($\Delta d = 0.5\mu$) in ocular reading, for two given hardness ranges:

<u>Load g</u>	<u>error %</u>	
	<u>At VHN 100</u>	<u>At VHN 800</u>
100	+ 2	+ 8
50	+ 3	+ 10
10	+ 10	+ 30

Since most of the experimental errors tend to raise the apparent hardness, the hardness seems to increase with decreasing load. In order to obtain the smallest error possible in the present experiments, a 50 g load was used in preference. This was the maximum load which satisfied the practical rule that the impression diameter should be not greater than 1/5 of the diameter of the constituent. In certain cases, however, this load was too large and 10 g load had to be used. Microhardness readings obtained with these two loads on the same specimens compare in the following way:

Spec. No.	Cu rich constituent			Fe rich constituent		
	L ₁ = 10g	L ₂ = 50g	L ₁ /L ₂	L ₁ = 10g	L ₂ = 50g	L ₁ /L ₂
28	126	118	1.07	143	122	1.17
61b	106	95	1.12	172	143	1.20
66b	111	93	1.19	-	-	-
67	115	110	1.05	201	169	1.19
73	95	86	1.10	140	124	1.13
78	120	111	1.08	-	-	-
81	90	86	1.05	-	-	-

On the average the 10 g load gave 9% higher readings for the copper-rich constituent and 17% higher for the iron-rich constituent than the 50 g load.

APPENDIX II

Processing and Tensile Data

Spec. No.	Fe Powder Mesh Size	Compact. Pressure psi.	Sintered Density %	Infiltration		Infilt. Density %	Tensile Properties		
				Temp. °C	Time min.		YS psi.	UTS psi.	E %
12	-80 +150	30,000	75.0	1150	10	-	18,900	32,000	8.0
13	"	"	77.0	"	"	-	21,000	33,400	10.0
16	"	20,000	68.6	"	"	-	16,200	32,800	8.5
17	"	"	68.8	"	"	-	16,800	40,300	25.0
18	"	"	69.4	"	"	-	17,700	40,800	28.0
19	-100 +150	30,000	72.8	"	"	-	21,200	45,600	25.0
23	-200 +270	"	77.8	"	200	98.15	54,500	59,700	4.5
24	"	"	77.4	"	"	-	54,600	67,200	3.5
25	"	"	79.5	"	"	98.48	54,700	62,700	3.5
26	"	"	77.4	"	10	97.89	17,000	38,400	9.6
27	"	"	78.8	"	"	98.15	20,900	38,300	7.0
28	"	"	77.7	"	"	97.99	20,000	39,100	9.4
29	"	"	-	"	60	-	33,500	46,800	7.0
31	"	"	78.5	"	"	98.42	28,200	45,500	7.0
36	"	nil	63.3	"	10	97.96	23,200	37,300	7.5
37	"	"	62.6	"	"	97.67	25,100	28,500	3.0
38	"	"	59.8	"	"	-	23,200	43,200	5.0
39	"	20,000	69.8	"	"	97.32	23,000	32,400	3.5
40	"	"	70.7	"	"	-	23,800	40,000	8.0
41	"	"	74.7	"	"	97.88	20,900	35,500	8.0
42	"	30,000	77.3	1260	"	-	32,300	46,800	3.0
43	"	"	77.4	"	"	97.94	51,800	51,800	0
44	"	"	77.2	"	"	98.27	36,700	52,400	8.0
45	"	"	78.0	1100	"	97.64	18,600	40,800	16.0
46	"	"	78.3	"	"	96.84	18,800	37,000	13.5
47	"	"	78.6	"	"	95.79	18,400	35,700	9.5
48	-100 +150	"	76.0	1150	"	97.58	21,900	45,400	16.0
49	"	"	76.0	"	"	96.69	19,900	42,200	23.0
50	"	"	75.8	"	"	96.91	20,900	41,300	12.0 20.0

* ...

... continued

Appendix II (Continued)

Spec. No.	Fe Powder Mesh Size	Compact. Pressure psi.	Sintered Density %	Infiltration		Infilt. Density %	Tensile Properties		
				Temp. °C	Time °C		YS psi.	UTS psi.	E %
51	-150 +200	30,000	77.3	1150	10	97.76	20,500	38,000	18.5*
52	"	"	76.6	"	"	96.97	19,000	38,000	16.5
53	"	"	77.3	"	"	97.65	23,200	41,300	17.5
55	-270 +325	"	75.4	"	"	97.52	23,600	46,600	12.0*
57	-325	"	74.0	"	"	97.47	27,500	37,400	5.0
59	-200 +275	"	75.0	"	420	98.16	56,100	66,900	1.0
61b	"	nil	60.2	"	120	98.36	35,200	42,200	4.0
62c	"	"	58.2	"	"	98.25	30,300	41,300	1.0*
66b	"	20,000	71.4	"	"	98.05	45,600	50,700	2.0
67	"	30,000	77.3	"	"	97.82	42,000	52,800	5.0
69	"	"	75.8	"	"	97.73	36,000	48,400	4.0
73	-100 +150	"	74.0	"	"	98.21	36,400	53,300	7.5
74	"	"	73.7	"	"	98.02	35,800	47,600	4.5
75	"	"	74.2	"	"	98.58	39,500	45,400	2.0
77	-200 +270	"	77.6	1370	10	97.56	46,800	54,500	2.0
78	"	"	76.9	"	"	97.79	53,200	60,800	2.0
79	"	"	76.2	"	"	97.74	62,300	62,300	0
85	-270 +325	"	76.2	1150	120	97.90	41,100	41,300	0.5
86	-325	"	79.8	"	"	99.20	40,200	40,400	0.5
89	-200 +270	"	77.2	"	300	98.50	55,300	64,700	4.0
90	"	"	76.9	"	"	98.10	57,700	57,700	0

*Specimens broke outside gauge mark

APPENDIX III

Metallographic Measurements

Spec. No.	Vol.% copper	Diameter of Iron part. μ	Mean Free Path μ	Inter particle spacing, μ	Microhardness, VHN	
					Fe rich phase	Cu rich phase
19	20.7	91.6	24.0	115.6	118	114
25	19.6	53.5	13.0	66.5	204	117
28	19.6	48.7	11.8	60.5	122	118
31	21.3	50.2	13.7	63.9	137	117
36	39.9	43.2	28.7	71.9	145*	106*
39	27.7	47.9	18.5	66.4	148*	105*
40	(25.4)	43.8	14.9	58.7	103	-
44	19.7	51.3	12.6	63.9	140	118
46	23.5	46.7	14.3	61.0	118	110
50	22.3	81.0	23.2	104.2	148*	92*
53	23.2	58.8	17.7	76.5	143*	106*
55	24.0	37.9	11.9	49.8	153*	111*
57	21.5	21.7	6.0	27.7	154*	117*
59	24.0	52.9	16.8	69.7	206	111
61b	37.7	44.7	27.3	72.0	143	95
66b	26.0	46.3	16.2	62.5	118	93
67	19.9	52.6	13.1	65.7	169	110
73	24.5	92.7	30.2	122.5	124	86
78	20.9	50.1	13.2	63.3	165	111
85	25.3	40.9	13.8	54.7	197*	105*
86	21.5	34.3	9.3	43.7	229*	125*
89	25.4	53.9	18.3	72.2	203	112

* tests with 10 g load, while the rest with 50 g load

VII. BIBLIOGRAPHY

1. Elliot, J.E., Metallurgia 52, (1955) 226-234.
2. "Metals Handbook", 1948 edition, A.S.M.
3. Whalen, T.G., Humenik, M., Proc. 18th Ann. Powder Met. Conf. 18 (1962) 85.
4. Kingery, W.D., J. Appl. Phys. 30, 3 (1959) 301.
5. Inman, M., Met. Review 8, 30 (1963) 120.
6. Taylor, J.W., Progress in Nucl. En. Series 5, 2 (1959) 398.
7. Swalin, R.A., "Thermodynamics of Solids" (1962), John Wiley and Sons, New York, 205.
8. Barrett, C.S., "Structure of Metals" (1952), McGraw-Hill, New York, 350.
9. Edelson, B.I., Baldwin, W.M., Trans. Quart. A.S.M. 55 1 (1962) 230-250.
10. Krock, R.H., Shepard, L.A., Trans. A.I.M.E. 227 (1963) 1127.
11. Gregory, E., Grant, N.J., Trans. A.I.M.E. February (1954) 247.
12. Pines, B.Y., Sukhinin, N.I., J. Tech. Phys. U.S.S.R. 26 (1956) 2076.
13. Teodorovich, O.K., Radomyselsky, I.O., Poroskovaya Metallurgia, U.S.S.R. 4 (1961) 63.
14. Kimura, T., Planseeberichte fur Pulvermet 7, 2 (1959) 50.
15. Goetzel, C.G., Product Eng. 18 (1947) 115.
16. Heheman, R.F., Luhan, V.J., Troiano, A.R., Trans. A.S.M. 49 (1957) 409.
17. Kopecki, E.S., Iron Age 157 (1946) 50.
18. Kelley, F.C., Iron Age 157 (1946) 57.
19. Northcott, L., Loadbeater, C.J., Special Report No. 38, Iron and Steel Ins. (1947) 142.
20. Smith, C.S. Palmer, E.W., J. Metals 188 12 (1950) 1486.
21. Rennhack, E.H., Proc. 17th Annual Powder Met. Conf. 17 (1961) 12.
22. Teodorovich, O.K., Frantzevich, I.N., Porosk, Met. U.S.S.R. 6 (1961).
23. Goetzel, C.G., "Treatise on Powder Metallurgy" 2 (1950) Interscience.

24. Schwartzkopf, P., Met. Progress 57 (1950) 64.
25. Gurland, J., Norton, J.T., J. Metals 4 (1952) 1051.
26. Hames, F.A., Gertsman, S.L., Int. Report, Dept. of Mines, PMI 6124 (1961).
27. Frantzevich, I.N., Teodorovich, O.K., Metallobed. i. Obr. Met. U.S.S.R. 2
(1958) 20.
28. Underwood, E.E., Met. Eng. Quart. 1 3,4 (1961).
29. Fullman, R.L., Trans. A.I.M.E. 197 (1953) 447.
30. Semlak, K.A., Rhines, F.N., Trans. A.I.M.E. 212 (1958) 325.
31. Kuzmik, J.F., Mazza, E.N., J. Metals, October (1950) 1218.
32. Price, G.H., Smithells, C.J., Williams, S.V., J. Inst. of Met. 62 (1938) 239.
33. Bredzs, N., Schwartzbart, H., Suppl. Welding J. August (1959).
34. Lenel, F.V., Ansell, G.S., Proc. Powder. Met. Conf., New York (1960) 267.
35. Buckler, H., Proc. Powder Met. Conf., New York (1960) 221.